IMAGING SCHEMES FOR CRACKS AND INCLUSIONS*

H. AMMARI†, J. GARNIER‡, H. KANG§, W.-K. PARK¶, AND K. SØLNA‖

Abstract. We consider the problem of locating defects and estimating their geometric features from multi-static response matrix measurements at single or multiple frequencies. A main objective is to design specific defect detection rules and to analyze their receiver operating characteristics and the associated resolution and signal-to-noise ratio. In this paper we introduce a unified analytic framework that uses high-frequency asymptotic methods in combination with a hypothesis test based formulation to construct specific procedures for detection and characterization of cracks and inclusions. A central ingredient in our approach is the use of random matrix theory to characterize the signal space associated with the multi-static response matrix measurements. We present numerical experiments to illustrate some of our main findings.

Key words. crack and inclusion detections, asymptotic imaging, imaging algorithms, random matrices, measurement noise, Berens' modelling, hypothesis testing, probability of detection

AMS subject classifications. 78M35, 78A46, 15B52

1. Introduction. The focus of this paper is on imaging small defects from measurements at single or multiple frequencies. Two different types of defects are considered: cracks and inclusions. Our general imaging approach is based on relatively high-frequency asymptotic formulas for the signature of the defect.

We assume that we have coincident transmitter and receiver arrays of n elements. The multi-static response (MSR) matrix is the transmit-receive responses of this array. The problem we consider is to image the defect from the MSR matrix measurements at single or multiple frequencies in the presence of measurement noise.

We construct different imaging functionals for imaging the defects from MSR measurements at a single or multiple frequencies. In particular, MUSIC (which stands for MUltiple SIgnal Classification) and Kirchhoff-type algorithms are investigated. Applying the techniques of statistical hypothesis testing we derive a strategy for ruling on the presence/absence of a defect based on the introduced imaging functionals. We also introduce the notion of resolution, which takes into account the signal-to-noise-ratio (SNR), and analyze the resolution-enhancement effect obtained with broadband signals. We revisit Berens' modelling that was introduced in [11] and derive, using our asymptotic formulas for the signature of the defect, appropriate probability of detection functions. The detailed statistical analysis carried out in this paper shows that the probability of false alarm is given in terms of a Tracy-Widom distribution, which is a bell-shape function somewhat different from the Gaussian distribution usually applied. Finally we perform numerical experiments using the proposed algorithms to test their performance and efficiency.

The paper presents a unified framework for imaging defects. It proposes efficient imaging algorithms and establishes an approach for hypothesis testing and resolution analysis. The paper extends several recent results, concepts, and methods for imaging defects. In [9] a continuous model was considered and an asymptotic

*This work was supported by the Agence Nationale de la Recherche, NRF20090085987, KRF-2008-220-C00002, and NSF grant DMS0709389.

† Institut Langevin, CNRS UMR 7587, ESPCI, 10 rue Vauquelin, 75231 Paris Cedex 05, France (habib.ammari@espci.fr).

‡Laboratoire de Probabilités et Modèles Aléatoires & Laboratoire Jacques-Louis Lions, Université Paris VII, 2 Place Jussieu, 75251 Paris Cedex 5, France (garnier@math.jussieu.fr).

§Department of Mathematics, Inha University, Incheon 402-751, Korea (hbkang@inha.ac.kr).

¶Department of Mathematics, Kookmin University, Seoul 136-702, Korea (parkwk@kookmin.ac.kr).

‖Department of Mathematics, University of California, Irvine, CA 92697 (ksolna@math.uci.edu).

expansion of the boundary perturbations that are due to the presence of a small crack was derived. Moreover, a MUSIC-type approach for locating the crack from boundary measurements at a single frequency was designed. It was also shown that the location and the length of the crack can be estimated from the projection onto the noise space and the first significant singular value of the response matrix while the direction of the crack can only be estimated from the second singular vector. In [4, 5] a MUSIC-type imaging of small inclusions at a single frequency in the discrete framework has been presented. High-frequency asymptotic formulas for the perturbations in the MSR measurements due to small inclusions have been derived in [3, 22] and time-reversal techniques studied in [3]. In [19], a notion of resolution for imaging point sources has been introduced and a resolution analysis successfully carried out in the presence of noise. In this paper we integrate and extend these techniques by introducing an analytic framework that uses high-frequency asymptotic methods in combination with a hypothesis test based formulation to construct specific procedures for detection and characterization of cracks and inclusions. A central ingredient in our approach is the use of random matrix theory to characterize the signal space associated with the MSR measurements.

The paper is organized as follows. In Section 2 an asymptotic formalism for defect imaging is established. We consider two principal situations, either with cracks or inclusions. Motivated by this description imaging functionals to locate the defects are introduced in Section 3. Then, we present the test for detection of the crack or inclusion, that is to rule on whether they are present or not. This crucial test is based on analysis of the singular values of the response matrix and is derived in Section 4. An extension of Berens' modelling for defect detection is given in Section 4.5. In Section 5 we use the singular vectors to estimate the location given that there is a crack present. In the location estimation we introduce a location dependent threshold to the test whether a search point is associated with a defect or not. A resolution analysis is carried out in Section 6. In Section 7, optimization algorithms for reconstructing the crack orientation or the inclusion polarization tensor are presented. We illustrate with some numerical examples in Section 8. The paper ends with a discussion in Section 9. Some background on the probabilistic framework together with a proof of the asymptotic expansion of the effect of a small crack are given in the appendices.

For the sake of simplicity, we only consider the two-dimensional imaging problem but stress that the techniques developed here apply directly to the three-dimensional case.

2. Asymptotic Formalism.

2.1. Asymptotic Modelling of Cracks. We shall first consider the case where the defect is a small perfectly conducting crack. The crack Σ_ε is characterized by its size ε, location $\boldsymbol{x}^c$, and orientation $\boldsymbol{t}$ and we consider two space dimensions so that the crack is a line.

We assume a transducer array with the transducers located at $(\boldsymbol{x}_j = (x_1^{(j)}, 0); j = 1, \ldots, n)$, moreover, that the full response matrix is available. First, we assume that there is no noise. The governing equation for the time-harmonic field $u_\varepsilon^{(j)}$ emitted by a source at $\boldsymbol{x}_j$ is

$$\begin{cases} \Delta u_\varepsilon^{(j)} + \dfrac{\omega^2}{c_0^2} u_\varepsilon^{(j)} = \delta_{\boldsymbol{x}_j} \quad \text{in } \mathbb{R}^2 \setminus \overline{\Sigma_\varepsilon}, \\ u_\varepsilon^{(j)} = 0 \quad \text{on } \Sigma_\varepsilon, \\ \left| \Big(\dfrac{\partial}{\partial |\boldsymbol{x}|} - i \dfrac{\omega}{c_0} \Big) \Big(u_\varepsilon^{(j)}(\boldsymbol{x}) - \hat{G}(\omega, \boldsymbol{x}, \boldsymbol{x}_j) \Big) \right| = \mathrm{O}(|\boldsymbol{x}|^{-3/2}), \end{cases} \tag{2.1}$$

where $\hat{G}$ is the time-harmonic Green function

$$\hat{G}(\omega,\boldsymbol{x},\boldsymbol{y}) = \frac{i}{4}H_0^{(1)}\Big(\frac{\omega}{c_0}|\boldsymbol{y}-\boldsymbol{x}|\Big), \tag{2.2}$$

using the notation $|\boldsymbol{y}| = \|\boldsymbol{y}\|_2$. Here, $H_0^{(1)}$ is the zeroth order Hankel function of the first kind. Using the asymptotic form of the Hankel function

$$H_0^{(1)}(x) \simeq \sqrt{2/(\pi|x|)}\exp(ix - i\,\mathrm{sgn}(x)\pi/4) \quad \text{for } |x| \gg 1,$$

we find that for $\omega|\boldsymbol{x}-\boldsymbol{y}|/c_0 \gg 1$:

$$\hat{G}(\omega,\boldsymbol{x},\boldsymbol{y}) \simeq \frac{\sqrt{c_0}}{2\sqrt{2\pi}}\frac{\exp(i\,\pi/4)}{\sqrt{\omega|\boldsymbol{y}-\boldsymbol{x}|}}\exp\Big(i\frac{\omega}{c_0}|\boldsymbol{y}-\boldsymbol{x}|\Big), \tag{2.3}$$

and

$$\nabla\hat{G}(\omega,\boldsymbol{x}^c,\boldsymbol{x}_j) \simeq \frac{\sqrt{c_0}}{2\sqrt{2\pi}}\left(\frac{i\omega(\boldsymbol{x}^c-\boldsymbol{x}_j)}{c_0|\boldsymbol{x}^c-\boldsymbol{x}_j|}\right)\frac{\exp(i\,\pi/4)}{\sqrt{\omega|\boldsymbol{x}^c-\boldsymbol{x}_j|}}\exp\Big(i\frac{\omega}{c_0}|\boldsymbol{x}^c-\boldsymbol{x}_j|\Big).$$

We shall assume a high frequency regime with $\omega L/c_0 \gg 1$ for L the distance from the array center point to the crack center point. Regarding the crack size we assume

$$\frac{\omega\varepsilon}{c_0} < 1.$$

We define the response matrix entries by $A_{jl} := u_\varepsilon^{(j)}(\boldsymbol{x}_l)$. Following [9], we prove in Appendix B that the following asymptotic formula is valid for ω of order $o(\varepsilon)$:

$$\begin{aligned}
A_{jl}(\omega) = {}& \frac{2\pi\hat{G}(\omega,\boldsymbol{x}_j,\boldsymbol{x}^c)\hat{G}(\omega,\boldsymbol{x}^c,\boldsymbol{x}_l)}{\log(\frac{\omega\varepsilon}{2c_0})+\gamma-\log 2-\frac{i}{2}} \\
& -\pi\varepsilon^2\frac{\partial}{\partial t}\hat{G}(\omega,\boldsymbol{x}_j,\boldsymbol{x}^c)\frac{\partial}{\partial t}\hat{G}(\omega,\boldsymbol{x}^c,\boldsymbol{x}_l) + \mathrm{o}\Big(\frac{\varepsilon^2\omega^2}{c_0^2}\Big) \\
= {}& \frac{ic_0}{4\omega\sqrt{|\boldsymbol{x}_j-\boldsymbol{x}^c||\boldsymbol{x}_l-\boldsymbol{x}^c|}}\exp\left(\frac{i\omega}{c_0}(|\boldsymbol{x}_j-\boldsymbol{x}^c|+|\boldsymbol{x}_l-\boldsymbol{x}^c|)\right) \\
& \times\left[\frac{1}{\log(\frac{\omega\varepsilon}{2c_0})+\gamma-\log 2-\frac{i}{2}} - \frac{\varepsilon^2\omega^2}{2c_0^2}\frac{((\boldsymbol{x}_j-\boldsymbol{x}^c)\cdot\boldsymbol{t})((\boldsymbol{x}_l-\boldsymbol{x}^c)\cdot\boldsymbol{t})}{|\boldsymbol{x}_j-\boldsymbol{x}^c||\boldsymbol{x}_l-\boldsymbol{x}^c|}\right] \\
& +\mathrm{o}\Big(\frac{\varepsilon^2\omega^2}{c_0^2}\Big),
\end{aligned} \tag{2.4}$$

where $\gamma \simeq 0.577$ is the Euler constant and $\partial/\partial t$ stands for the tangential derivative.

2.2. Asymptotic Modelling of Inclusions. We consider next the (electromagnetic) situation where D is an inclusion with constant parameters $0 < \mu < +\infty$ and $0 < q < +\infty$, $(\mu, q) \neq (1, 1)$, located in a background medium with permeability and permittivity equal to 1.

Suppose that $D = \varepsilon B + \boldsymbol{x}^c$, where B is a domain which plays the role of a reference domain, ε denotes the small diameter of D, and $\boldsymbol{x}^c$ indicates the location of D.

Using the same notation as above, let $u_\varepsilon^{(j)}$ be the solution of

$$\begin{cases}
\nabla\cdot\Big(1+(\frac{1}{\mu}-1)\chi(D)\Big)\nabla u_\varepsilon^{(j)} + \dfrac{\omega^2}{c_0^2}(1+(q-1)\chi(D))u_\varepsilon^{(j)} = \delta_{\boldsymbol{x}_j} \quad \text{in } \mathbb{R}^2, \\
\left|\Big(\dfrac{\partial}{\partial|\boldsymbol{x}|}-i\dfrac{\omega}{c_0}\Big)\Big(u_\varepsilon^{(j)}(\boldsymbol{x})-\hat{G}(\omega,\boldsymbol{x},\boldsymbol{x}_j)\Big)\right| = \mathrm{O}(|\boldsymbol{x}|^{-3/2}),
\end{cases} \tag{2.5}$$

where $\hat{G}$ is the time-harmonic Green function (2.2). In [3] we proved that the following asymptotic of the response matrix entries holds:

$$\begin{aligned} A_{jl}(\omega) &= \varepsilon^2 \nabla \hat{G}(\omega, \boldsymbol{x}_j, \boldsymbol{x}^c) \cdot \mathbf{M}(\mu, B) \nabla \hat{G}(\omega, \boldsymbol{x}^c, \boldsymbol{x}_l) \\ &\quad - \frac{\varepsilon^2 \omega^2}{c_0^2} (q-1)|B| \hat{G}(\omega, \boldsymbol{x}_j, \boldsymbol{x}^c) \hat{G}(\omega, \boldsymbol{x}^c, \boldsymbol{x}_l) + \mathrm{o}\Big(\frac{\varepsilon^2 \omega^2}{c_0^2}\Big) \\ &= \frac{-i\omega\varepsilon^2}{8\pi c_0 \sqrt{|\boldsymbol{x}_j - \boldsymbol{x}^c||\boldsymbol{x}_l - \boldsymbol{x}^c|}} \exp\Big(i \frac{\omega}{c_0} (|\boldsymbol{x}_j - \boldsymbol{x}^c| + |\boldsymbol{x}_l - \boldsymbol{x}^c|)\Big) \\ &\quad \times \Big[\frac{(\boldsymbol{x}_j - \boldsymbol{x}^c) \cdot \mathbf{M}(\mu, B)(\boldsymbol{x}_l - \boldsymbol{x}^c)}{|\boldsymbol{x}_j - \boldsymbol{x}^c||\boldsymbol{x}_l - \boldsymbol{x}^c|} + |B|(q-1) \Big] + \mathrm{o}\Big(\frac{\varepsilon^2 \omega^2}{c_0^2}\Big), \end{aligned} \tag{2.6}$$

as $\omega \to +\infty$ and $\varepsilon\omega \to 0$. Here $\mathbf{M}(\mu, B)$ is the polarization tensor given by [6, 7]:

$$\mathbf{M}(\mu, B) := (\frac{1}{\mu} - 1) \int_B \nabla(\hat{\boldsymbol{v}}(\tilde{\boldsymbol{x}}) + \tilde{\boldsymbol{x}})\, d\tilde{\boldsymbol{x}},$$

where $\hat{\boldsymbol{v}}$ is the solution to

$$\begin{cases} \Delta \hat{\boldsymbol{v}} = \mathbf{0} \quad \text{in } \mathbb{R}^2 \setminus \overline{B}, \\ \Delta \hat{\boldsymbol{v}} = \mathbf{0} \quad \text{in } B, \\ \hat{\boldsymbol{v}}|_- - \hat{\boldsymbol{v}}|_+ = \mathbf{0} \quad \text{on } \partial B, \\ \dfrac{1}{\mu} \dfrac{\partial \hat{\boldsymbol{v}}}{\partial \nu}\Big|_- - \dfrac{\partial \hat{\boldsymbol{v}}}{\partial \nu}\Big|_+ = (\dfrac{1}{\mu} - 1)\nu \quad \text{on } \partial B, \\ \hat{\boldsymbol{v}}(\tilde{\boldsymbol{x}}) = O(|\tilde{\boldsymbol{x}}|^{-2}) \quad \text{as } |\tilde{\boldsymbol{x}}| \to +\infty, \end{cases}$$

with ν the outward-pointing unit normal vector.

Note that if the background medium is not the free-space then we have to replace, in the asymptotic formulas (2.4) and (2.6), the Green function $\hat{G}$ by the one associated with the background medium, $\hat{\mathcal{G}}$, and change the constant $\log(\frac{\omega\varepsilon}{2c_0}) + \gamma - \log 2 - \frac{i}{2}$ in formula (2.4) by

$$\log(\frac{\varepsilon}{2}) + 2\pi R(\omega, \mathbf{0}, \mathbf{0}),$$

where $R(\omega, \boldsymbol{x}, \boldsymbol{y}) = \hat{\mathcal{G}}(\omega, \boldsymbol{x}, \boldsymbol{y}) - \frac{1}{2\pi} \log|\boldsymbol{x} - \boldsymbol{y}|$.

3. Imaging Functionals.

3.1. Estimation of Crack Location. We consider first the case with cracks and recall some common imaging functionals, which are functions of a search point in the search domain where we are looking for defects. In Section 5 we shall relate this to a location-dependent test that is derived in a probabilistic framework.

Note that in the presence of one defect at $\boldsymbol{x}^c$ the response matrix has the approximate form

$$\mathbf{A} \simeq \tau(\omega, \boldsymbol{x}^c) \boldsymbol{d}(\omega, \boldsymbol{x}^c) \boldsymbol{d}(\omega, \boldsymbol{x}^c)^T, \tag{3.1}$$

with $\boldsymbol{d}(\omega, \boldsymbol{x}^c)$ the normalized illumination vector

$$\boldsymbol{d}(\omega, \boldsymbol{x}^c) = \frac{1}{\sqrt{\sum_{j=1}^n \frac{1}{|\boldsymbol{x}_j - \boldsymbol{x}^c|}}} \Big(\frac{1}{\sqrt{|\boldsymbol{x}_j - \boldsymbol{x}^c|}} \exp\Big(\frac{i\omega}{c_0} |\boldsymbol{x}_j - \boldsymbol{x}^c|\Big) \Big)_{j=1,\ldots,n} \tag{3.2}$$

and τ given by

$$\tau(\omega, \boldsymbol{x}^c) = \frac{i c_0 \sum_{j=1}^n \frac{1}{|\boldsymbol{x}_j - \boldsymbol{x}^c|}}{4\omega \Big(\log(\frac{\omega\varepsilon}{2c_0}) + \gamma - \log 2 - \frac{i}{2} \Big)}. \tag{3.3}$$

Here T denotes the transpose. The first singular value and singular vectors of the Singular Value Decomposition (SVD) of the data

$$\mathbf{A} = \mathbf{U}\mathbf{\Sigma}\overline{\mathbf{V}}^T,$$

satisfy $\mathbf{A}\boldsymbol{v}_1 = \sigma_1\boldsymbol{u}_1$ with the relations

$$\boldsymbol{u}_1 \simeq \exp(i\theta_1)\boldsymbol{d}, \quad \boldsymbol{v}_1 \simeq \exp(-i\theta_2)\overline{\boldsymbol{d}}, \quad \sigma_1 \simeq |\tau(\omega, \boldsymbol{x}^c)|, \tag{3.4}$$

with $\theta_1 + \theta_2 = \arg(\tau(\omega, \boldsymbol{x}^c))$.

A MUSIC imaging functional at a single frequency ω is given by

$$\mathcal{I}_{\mathrm{MU}}(\omega, \boldsymbol{x}^S) = \frac{1}{\left|\boldsymbol{d}(\omega, \boldsymbol{x}^S) - \big(\boldsymbol{u}_1(\omega), \boldsymbol{d}(\omega, \boldsymbol{x}^S)\big)\boldsymbol{u}_1(\omega)\right|}, \tag{3.5}$$

where $(\boldsymbol{a}, \boldsymbol{b}) = \overline{\boldsymbol{a}} \cdot \boldsymbol{b}$. We contrast this with a more classical Kirchhoff migration formulation which migrates traces to the search point $\boldsymbol{x}^S$:

$$\mathcal{I}_{\mathrm{KM}}(\omega, \boldsymbol{x}^S) = \overline{\boldsymbol{d}(\omega, \boldsymbol{x}^S)}^T \mathbf{A}(\omega)\overline{\boldsymbol{d}(\omega, \boldsymbol{x}^S)}. \tag{3.6}$$

In terms of the SVD decomposition of the response matrix the Kirchhoff migration functional can be written as

$$\mathcal{I}_{\mathrm{KM}}(\omega, \boldsymbol{x}^S) = \sum_{l=1}^{n} \big(\boldsymbol{d}(\omega, \boldsymbol{x}^S), \boldsymbol{u}_l(\omega)\big)\, \big(\boldsymbol{d}(\omega, \boldsymbol{x}^S), \overline{\boldsymbol{v}_l}(\omega)\big)\, \sigma_l(\omega). \tag{3.7}$$

In the case with one (sufficiently small) defect we have $\sigma_1 \gg \sigma_l$, for all $l = 2, \ldots, n$, and

$$\mathcal{I}_{\mathrm{KM}}(\omega, \boldsymbol{x}^S) \simeq \big(\boldsymbol{d}(\omega, \boldsymbol{x}^S), \boldsymbol{u}_1(\omega)\big)\, \big(\boldsymbol{d}(\omega, \boldsymbol{x}^S), \overline{\boldsymbol{v}_1}(\omega)\big)\, \sigma_1(\omega). \tag{3.8}$$

With measurements of the response matrix at multiple frequencies, $(\omega_k)_{k=1,\ldots,K}$, we can construct the imaging functional by summing over frequencies

$$\mathcal{I}_{\mathrm{KMF}}(\boldsymbol{x}^S) = \frac{1}{K}\sum_{\omega_k} \overline{\boldsymbol{d}(\omega_k, \boldsymbol{x}^S)}^T\, \mathbf{A}(\omega_k)\overline{\boldsymbol{d}(\omega_k, \boldsymbol{x}^S)} \tag{3.9}$$

where K is the number of frequencies (ω_k). An alternative imaging functional when searching for a single defect is

$$\mathcal{I}_{\mathrm{MT}}(\boldsymbol{x}^S) = \frac{1}{K}\sum_{\omega_k} \big(\boldsymbol{d}(\omega_k, \boldsymbol{x}^S), \boldsymbol{u}_1(\omega_k)\big)\, \big(\boldsymbol{d}(\omega_k, \boldsymbol{x}^S), \overline{\boldsymbol{v}_1}(\omega_k)\big) \tag{3.10}$$

in which we have renormalized the information provided by the different modes, yet retained phase coherency. Finally, it is also possible to use a matched field imaging functional:

$$\mathcal{I}_{\mathrm{MF}}(\boldsymbol{x}^S) = \frac{1}{K}\sum_{\omega_k} \left|\overline{\boldsymbol{d}(\omega_k, \boldsymbol{x}^S)}^T\, \mathbf{A}(\omega_k)\overline{\boldsymbol{d}(\omega_k, \boldsymbol{x}^S)}\right|^2 \tag{3.11}$$

in which the phase coherence between the different frequency-dependent components is not exploited. As we will see in Section 5, this makes sense when the different frequency-dependent components are incoherent.

3.2. Estimation of Inclusion Location. Define the $n \times 3$ matrix $\mathbf{d}(\omega, \boldsymbol{x}^S)$ by

$$\mathbf{d}(\omega, \boldsymbol{x}^S) = \frac{1}{\sqrt{\sum_{j=1}^n \frac{|(1, \boldsymbol{x}_j - \boldsymbol{x}^S)|^2}{|\boldsymbol{x}_j - \boldsymbol{x}^S|}}} \left(\frac{\left(1, (\boldsymbol{x}_j - \boldsymbol{x}^S)^T\right)}{\sqrt{|\boldsymbol{x}_j - \boldsymbol{x}^S|}} \exp\left(i \frac{\omega}{c_0} |\boldsymbol{x}_j - \boldsymbol{x}^S|\right) \right)_{j=1,\ldots,n} \tag{3.12}$$

Let $\mathbf{A} = \mathbf{U}\mathbf{\Sigma}\overline{\mathbf{V}}^T$ be the SVD of the matrix $\mathbf{A}$. The rank of $\mathbf{A}$ is three times the number of inclusions (if for any inclusion its permittivity and permeability are different from 1) [4, 5]. In the case of a unique inclusion the first three columns of $\mathbf{U}$ provide an orthonormal basis for the image space of $\mathbf{A}$ which is denoted by the $n \times 3$ matrix $\mathbf{U}_S$. The $n \times n$ matrix $\mathbf{P_A} = \mathbf{U}_S \overline{\mathbf{U}}_S^T$ is the orthogonal projection onto the image space of the response matrix $\mathbf{A}$.

A MUSIC imaging functional at a single frequency ω is then given by [4, 5]:

$$\mathcal{I}_{\mathrm{MU}}(\boldsymbol{x}^S) = \frac{1}{\left|(\mathbf{I} - \mathbf{P_A})\mathbf{d}(\omega, \boldsymbol{x}^S)\right|} = \frac{1}{\left|\mathbf{d}(\omega, \boldsymbol{x}^S) - \sum_{l=1}^3 \boldsymbol{u}_l(\omega) \overline{\boldsymbol{u}_l(\omega)}^T \mathbf{d}(\omega, \boldsymbol{x}^S)\right|}, \tag{3.13}$$

where $\mathbf{I}$ is the $n \times n$ identity matrix and $(\boldsymbol{u}_l)_{l=1,\ldots,3}$ are the right singular vectors of $\mathbf{A}$.

In the case of measurements at multiple frequencies (ω_k), we may construct the imaging functional as

$$\mathcal{I}_{\mathrm{MT}}(\boldsymbol{x}^S) = \frac{1}{K} \sum_{\omega_k} \sum_{l=1}^3 \left(\boldsymbol{d}(\omega_k, \boldsymbol{x}^S), \boldsymbol{u}_l(\omega_k)\right) \left(\boldsymbol{d}(\omega_k, \boldsymbol{x}^S), \overline{\boldsymbol{v}_l}(\omega_k)\right), \tag{3.14}$$

where K is the number of frequencies and $(\boldsymbol{v}_l)$ are the left singular vectors of $\mathbf{A}$. In the following sections we shall introduce tests deriving from a hypothesis test based framework to quantify when one can actually detect a defect.

4. Optimal Detection.

4.1. Singular Values of Noisy Response Matrices. In this subsection we consider the case in which the MSR matrix is obtained in the absence of any crack or inclusion so that it contains only noisy data coming primarily from electronic noise. Therefore, we assume that the MSR matrix $\mathbf{A}$ is random with complex Gaussian statistics. In other words the entries A_{jl}, $1 \leq j, l \leq n$, are modelled as independent complex Gaussian random variables with mean zero and variance a^2/n (equivalently $\mathbf{A} = \mathbf{A}_r + i\mathbf{A}_i$ with $\mathbf{A}_r$ and $\mathbf{A}_i$ two independent real Gaussian matrices whose entries have mean 0 and variance $a^2/(2n)$).

4.1.1. Spectral Measure. We denote by $\sigma_1^{(n)} \geq \sigma_2^{(n)} \geq \sigma_3^{(n)} \geq \cdots \geq \sigma_n^{(n)}$ the singular values of the response matrix $\mathbf{A}$ sorted by decreasing order. We introduce the corresponding spectral measure:

$$N^{(n)}([\sigma_u, \sigma_v]) = \frac{1}{n} \mathrm{Card}\left\{ j \in \{1, \ldots, n\},\, \sigma_j^{(n)} \in [\sigma_u, \sigma_v] \right\}, \text{ for any } \sigma_u < \sigma_v.$$

$N^{(n)}$ is a counting measure which consists of a sum of Dirac masses:

$$N^{(n)} = \frac{1}{n} \sum_{j=1}^n \delta_{\sigma_j^{(n)}}.$$

The following result is standard in Random Matrix Theory [27]:

PROPOSITION 4.1. *When $n \to \infty$ the spectral measure $N^{(n)}$ almost surely converges to the absolutely continuous measure N with compact support:*

$$N([\sigma_u, \sigma_v]) = \int_{\sigma_u}^{\sigma_v} \rho(\sigma) d\sigma,$$

where

$$\rho(\sigma) = \frac{1}{\sigma_c} \rho_{sc}\Big(\frac{\sigma}{\sigma_c}\Big), \qquad \rho_{sc}(\sigma) = \begin{cases} \frac{1}{\pi}\sqrt{4-\sigma^2} & \text{if } 0 < \sigma \leq 2, \\ 0 & \text{otherwise,} \end{cases} \tag{4.1}$$

and $\sigma_c = a$.

The function ρ is the asymptotic spectral measure: $\rho(\sigma)d\sigma$ gives the proportion of singular values of the response matrix that lie in the elementary interval $[\sigma, \sigma+d\sigma]$. The normalized function ρ_{sc} is the semi-circle law.

4.1.2. Moments. In the asymptotic regime $n \to \infty$ we have

$$\frac{1}{n}\sum_{j=1}^{n} (\sigma_j^{(n)})^{2k} = \int_0^\infty \sigma^{2k} \rho(\sigma) d\sigma = \gamma_{sc}^{(2k)} \sigma_c^{2k}, \tag{4.2}$$

$$\gamma_{sc}^{(2k)} = \int_0^\infty \sigma^{2k} \rho_{sc}(\sigma) d\sigma, \tag{4.3}$$

with $\gamma_{sc}^{(2)} = 1$, $\gamma_{sc}^{(4)} = 2$, $\gamma_{sc}^{(6)} = 5$. We can describe the fluctuations of the second moment which has Gaussian distribution with a relative amplitude of the order of n^{-1}:

$$\begin{aligned} \frac{1}{n}\sum_{j=1}^{n} (\sigma_j^{(n)})^2 &= \frac{1}{n}\mathrm{Trace}\big(\overline{\mathbf{A}}^T \mathbf{A}\big) = \frac{1}{n}\sum_{j,l=1}^{n} |A_{jl}|^2 \\ &\overset{dist.}{=} \sigma_c^2 + \frac{\sigma_c^2}{n}\mathcal{N}(0,1), \end{aligned} \tag{4.4}$$

when n is large (note that $\mathbb{E}(|A_{jl}|^2) = a^2$ and $\mathrm{Var}\big(|A_{jl}|^2\big) = a^4$). Here $\mathbb{E}$ stands for the expectation (mean value), Var for the variance, $\mathcal{N}(\mu, \sigma^2)$ for the normal distribution with mean μ and variance σ^2, and $\overset{dist.}{=}$ means "equal in distribution".

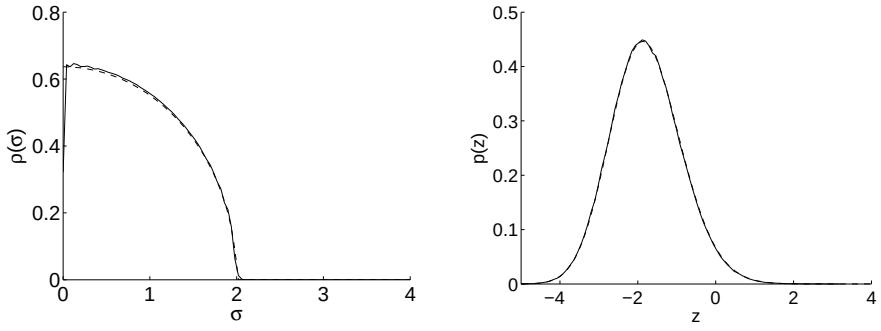

FIG. 4.1. *Left figure: spectral measure for a complex Gaussian random matrix with $\sigma_c = 1$ obtained from Monte Carlo simulations with $n = 50$ (solid) and compared with the theoretical semi-circle law (dashed). Right figure: probability density function of the normalized maximal singular value $Z_2 = 2^{2/3} n^{2/3} (\max \sigma_j^{(n)}/\sigma_c - 2)$ obtained from Monte Carlo simulations with $n = 50$ (solid) and compared with the theoretical Tracy-Widom distribution of type 2 (dashed).*

4.1.3. Maximal Singular Value. The largest singular value is $2\sigma_{\rm c}$ up to a random correction of order $\sigma_{\rm c} n^{-2/3}$:

$$\sigma_1^{(n)} \overset{dist.}{=} \sigma_{\rm c}\big[2 + 2^{-2/3} n^{-2/3} Z_2 + o(n^{-2/3})\big]. \tag{4.5}$$

The random correction Z_2 looks Gaussian (see Fig. 4.1), but it is not. It is a Tracy-Widom distribution of type $\beta = 2$ [23]:

$$\mathbb{P}(Z_2 \leq z) = \int_{-\infty}^{z} p_{\rm TW2}(x)dx = \exp\Big(-\frac{1}{2}\int_z^{\infty}(x-z)\varphi^2(x)dx\Big),$$
$$\mathbb{E}(Z_2) \simeq -1.77, \qquad {\rm Var}(Z_2) \simeq 0.81,$$

with $\varphi(x)$ the solution of the Painlevé equation

$$\varphi''(x) = x\varphi(x) + 2\varphi(x)^3, \quad \varphi(x) \simeq {\rm Ai}(x),\ x \to \infty, \tag{4.6}$$

Ai being the Airy function.

Note that the random correction to the maximal singular value has a relative amplitude of the order of $n^{-2/3}$, while the random correction to the second moment (4.4) has a relative amplitude of order n^{-1}. Therefore, we obtain the following result:

PROPOSITION 4.2. *Let us consider the response matrix obtained with an electronic noise. The ratio of the first singular value over the L^2-norm of the other singular values*

$$R := \frac{\sigma_1^{(n)}}{\big(\frac{1}{n-1}\sum_{j=2}^{n}\big(\sigma_j^{(n)}\big)^2\big)^{1/2}} \tag{4.7}$$

has the following statistical distribution

$$R \overset{dist.}{=} 2 + \frac{1}{2^{2/3} n^{2/3}} Z_2, \tag{4.8}$$

when n is large, where Z_2 is a random variable independent of all the parameters which follows a Tracy-Widom distribution of type 2.

This result is very important. Combined with the corresponding result in the presence of a defect that we will present in Subsection 4.2, it allows us to build a likelihood-ratio test for the detection of a defect in the medium. By Neyman-Pearson Lemma [24] this test is of the form: when the ratio (4.7) is beyond a threshold value η (significantly larger than 2), then this means that a defect must be buried in the medium. The knowledge of the statistical distribution of the ratio (4.7) in the absence and in the presence of a defect will allow us to choose the threshold η to reach a prescribed level for the test (*i.e.*, a given probability of false alarm), and so that this test is the most powerful amongst all tests with this level (the power is the probability of detection); see Appendix A.

4.2. Singular Values of Noisy Response Matrices with a Crack. Here we consider the response matrix $\mathbf{A}$ obtained with a crack in the presence of additive electronic noise:

$$\mathbf{A} = \mathbf{A}_0 + \mathbf{W}, \tag{4.9}$$

where here $\mathbf{A}_0 = \boldsymbol{h}_0 \boldsymbol{h}_0^t$ is assumed to be a rank-one matrix and $\mathbf{W}$ is a complex Gaussian matrix as the one studied in Subsection 4.1. Let us denote by $\sigma_0 = \|\boldsymbol{h}_0\|_2^2$ the nonzero singular value of $\mathbf{A}_0$ and by $\sigma_1^{(n)} \geq \sigma_2^{(n)} \geq \sigma_3^{(n)} \geq \cdots \geq \sigma_n^{(n)}$ the singular values of the matrix $\mathbf{A}$. We introduce the parameter $\sigma_c = \sqrt{n}a$ where a^2 is

the variance of the entries of the matrix $\mathbf{W}$ which models additive electronic noise. For large n, we can expand the distribution of the singular values and we obtain the following results [15, 20]:

PROPOSITION 4.3.

a) *If $\sigma_c > \sigma_0$, then the largest singular value $\sigma_1^{(n)}$ obeys the same non-Gaussian statistics (with mean $2\sigma_c$) as in the absence of the crack.*

b) *If $\sigma_c < \sigma_0$, then the largest singular value $\sigma_1^{(n)}$ obeys Gaussian statistics with the mean and variance*

$$\mathbb{E}(\sigma_1^{(n)}) = \sigma_0 + \sigma_c^2\sigma_0^{-1}, \qquad \mathrm{Var}\big(\sigma_1^{(n)}\big) = \frac{1}{2n}\sigma_c^2\big(1 - \sigma_c^2\sigma_0^{-2}\big).$$

c) *For any σ_c the second singular value $\sigma_2^{(n)}$ is equal to $2\sigma_c$ up to a random correction that is of the order of $n^{-2/3}$ as $n \to \infty$.*

Several interesting features can be observed:

- The noise generates many small singular values, whose largest one is $\sigma_2^{(n)}$ which is of the order of $2\sigma_c$.
- The first singular value, $\sigma_1^{(n)}$, corresponding to the crack, increases as the noise increases. This is a manifestation of the level repulsion: the small singular values (and in particular $\sigma_2^{(n)}$) increase as the noise increases, and the strong singular value is repulsed.
- The first singular value, corresponding to the crack, and the second singular value, that is the largest singular value generated by the noise, are well separated as long as $\mathbb{E}(\sigma_1^{(n)}) > \mathbb{E}(\sigma_2^{(n)})$, *i.e.*, $\sigma_c < \sigma_0$. In the opposite case $\sigma_c > \sigma_0$ it is not possible to see the crack.

We can study the spectral measure of the $n-1$ smallest singular values $(\sigma_2^{(n)}, \sigma_3^{(n)}, \cdots, \sigma_n^{(n)})$:

$$N^{(n-1)}([\sigma_u, \sigma_v]) = \frac{1}{n-1}\mathrm{Card}\left\{j = 2, \ldots, n,\, \sigma_j^{(n)} \in [\sigma_u, \sigma_v]\right\}, \text{ for } \sigma_u < \sigma_v.$$

When n is large, $N^{(n-1)}$ is asymptotically equivalent to a continuous measure N compactly supported:

$$N([\sigma_u, \sigma_v]) = \int_{\sigma_u}^{\sigma_v} \rho(\sigma)d\sigma, \text{ with } \rho(\sigma) = \frac{1}{\sigma_c}\rho_{\mathrm{sc}}\Big(\frac{\sigma}{\sigma_c}\Big).$$

We can describe the ratio of the maximal singular value over the square root of the second moment by:

PROPOSITION 4.4. *Let us consider the response matrix obtained with a single crack in the presence of electronic noise. For $\sigma_c < \sigma_0$, the ratio (4.7) has the following statistical distribution*

$$R \overset{dist.}{=} \frac{\sigma_0}{\sigma_c} + \frac{\sigma_c}{\sigma_0} + \frac{1}{\sqrt{2n}}\sqrt{1 - \sigma_c^2\sigma_0^{-2}}\mathcal{N}(0,1). \tag{4.10}$$

For $\sigma_c > \sigma_0$ we have (4.8).

This proposition describes the statistical distribution of the ratio (4.7) in the presence of a crack. It allows us to compute explicitly the power of the likelihood-ratio test which is the most powerful test for a given false alarm rate by the Neyman-Pearson Lemma [16].

4.3. Singular Values of Symmetrized Noisy Response Matrices. In this section we assume that the response matrix is obtained in the presence of electronic noise only and that the matrix is symmetrized to reduce the noise variance of its off-diagonal entries. That is, the response matrix $\mathbf{A}$ is complex Gaussian

(with independent complex Gaussian entries with mean zero and variance a^2) and we consider the symmetrized matrix

$$\mathbf{A}^s = \frac{1}{2}\big(\mathbf{A} + \mathbf{A}^T\big).$$

Then the matrix $\mathbf{A}^s$ is symmetric complex and has random entries with Gaussian statistics: $A^s_{jl} = A^s_{lj}$ and the entries A^s_{jl}, $j \leq l$ are independent complex Gaussian random variables with mean zero and variance a_s^2/n off the diagonal ($j \neq l$) and $2a_s^2/n$ on the diagonal $j = l$, with $a_s = a/\sqrt{2}$. The symmetrization of the response matrix reduces the variance of its off-diagonal entries by a factor of $\sqrt{2}$.

We denote by $\sigma_1^{(n)} \geq \sigma_2^{(n)} \geq \sigma_3^{(n)} \geq \cdots \geq \sigma_n^{(n)}$ the singular values of the response matrix $\mathbf{A}^s$ sorted by decreasing order and by $N^{(n)}$ the corresponding spectral measure.

PROPOSITION 4.5. *When $n \to \infty$ the spectral measure $N^{(n)}$ almost surely converges to the absolutely continuous measure N with compact support:*

$$N([\sigma_u, \sigma_v]) = \int_{\sigma_u}^{\sigma_v} \rho(\sigma) d\sigma, \qquad \rho(\sigma) = \frac{1}{\sigma_{\rm c}^s} \rho_{\rm sc}\Big(\frac{\sigma}{\sigma_{\rm c}^s}\Big),$$

where $\rho_{\rm sc}$ is the semi-circle law given by (4.1) and $\sigma_{\rm c}^s = a_s = a/\sqrt{2}$.

In the asymptotic regime $n \to \infty$ the moments of the singular values are given by the formulas (4.2) with $\sigma_{\rm c}$ replaced by $\sigma_{\rm c}^s$. We can describe the fluctuations of the second moment which has Gaussian distribution with a relative amplitude of the order of n^{-1}:

$$\begin{aligned}\frac{1}{n}\sum_{j=1}^{n}(\sigma_j^{(n)})^2 &= \frac{1}{n}{\rm Trace}\big(\overline{(\mathbf{A}^s)}^T \mathbf{A}^s\big) = \frac{1}{n}\sum_{j,l=1}^{n} |A^s_{jl}|^2 \\ &\stackrel{dist.}{=} (\sigma_{\rm c}^s)^2 + \frac{(\sigma_{\rm c}^s)^2}{n}\mathcal{N}(1,2).\end{aligned}$$

when n is large (note that $\mathbb{E}(|A^s_{jj}|^2) = 2a_s^2$, ${\rm Var}\big(|A^s_{jj}|^2\big) = 4a_s^4$, $\mathbb{E}(|A^s_{jl}|^2) = a_s^2$, ${\rm Var}\big(|A^s_{jl}|^2\big) = a_s^4$, for $j \neq l$, and $\mathbf{A}^s$ is symmetric).

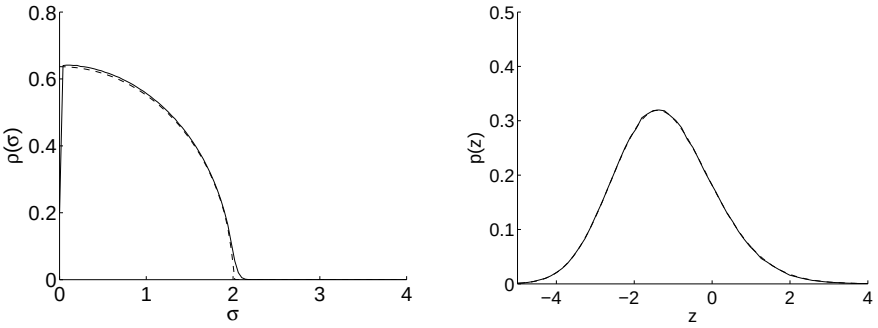

FIG. 4.2. *Left figure: spectral measure for a complex symmetric Gaussian random matrix with $\sigma_{\rm c} = 1$ obtained from Monte Carlo simulations with $n = 50$ (solid) and compared with the theoretical semi-circle law (dashed). Right figure: probability density function of the normalized maximal singular value $Z_1 = 2^{2/3} n^{2/3} (\max \sigma_j^{(n)}/\sigma_{\rm c}^s - 2)$ obtained from Monte Carlo simulations with $n = 50$ (solid) and compared with the theoretical Tracy-Widom distribution of type 1 (dashed).*

The largest singular value is $2\sigma_{\rm c}^s$ up to a random correction of order $\sigma_{\rm c}^s n^{-2/3}$:

$$\sigma_1^{(n)} \stackrel{dist.}{=} \sigma_{\rm c}^s\big[2 + 2^{-2/3} n^{-2/3} Z_1 + o(n^{-2/3})\big].$$

The random correction Z_1 looks Gaussian (see Fig. 4.2), but it is not. It is a Tracy-Widom distribution of type $\beta = 1$:

$$\mathbb{P}(Z_1 \leq z) = \int_{-\infty}^{z} p_{\mathrm{TW1}}(x)dx = \exp\Big(-\frac{1}{2}\int_{z}^{\infty} \varphi(x) + (x-z)\varphi^2(x)dx\Big),$$
$$\mathbb{E}(Z_1) \simeq -1.21, \qquad \mathrm{Var}(Z_1) \simeq 1.61,$$

where φ is the solution to (4.6).

Note that the random correction to the maximal singular value has a relative amplitude of the order of $n^{-2/3}$, while the random correction to the second moment has a relative amplitude of order n^{-1}. Therefore, we obtain the following result:

PROPOSITION 4.6. *Let us consider the symmetrized response matrix obtained in the presence of electronic noise. The ratio (4.7) has the following statistical distribution*

$$R \overset{dist.}{=} 2 + \frac{1}{2^{2/3}n^{2/3}} Z_1, \tag{4.11}$$

when n is large, where Z_1 is a random variable independent of all parameters following a Tracy-Widom distribution of type 1.

4.4. Singular Values of Symmetrized Response Matrices with a Crack. Here we consider the response matrix $\mathbf{A}$ given by (4.9) obtained with a single crack in the presence of additive electronic noise and we symmetrize this matrix:

$$\mathbf{A}^s = \frac{1}{2}\big(\mathbf{A} + \mathbf{A}^T\big) = \mathbf{A}_0 + \mathbf{W}^s,$$

where $\mathbf{W}^s$ is a complex symmetric Gaussian matrix like the one studied in Subsection 4.3. Let us denote by $\sigma_0 = \|\boldsymbol{h}_0\|_2^2$ the nonzero singular value of $\mathbf{A}_0$ and by $\sigma_1^{(n)} \geq \sigma_2^{(n)} \geq \sigma_3^{(n)} \geq \cdots \geq \sigma_n^{(n)}$ the singular values of the matrix $\mathbf{A}^s$. We introduce the parameter $\sigma_c^s = \sqrt{n/2}a$ where a^2 is the variance of the entries of the matrix $\mathbf{W}$ due to additive electronic noise. Let us denote by $\sigma_1^{(n)} \geq \sigma_2^{(n)} \geq \sigma_3^{(n)} \geq \cdots \geq \sigma_n^{(n)}$ the singular values of the response matrix $\mathbf{A}^s$. For large n, we can expand the distribution of the singular values and we get the following results:

PROPOSITION 4.7.

a) *If $\sigma_{\mathrm{c}}^s > \sigma_0$, then the largest singular value $\sigma_1^{(n)}$ obeys the same non-Gaussian statistics (with mean $2\sigma_c^s$) as in the absence of the crack.*

b) *If $\sigma_{\mathrm{c}}^s < \sigma_0$, then the largest singular value $\sigma_1^{(n)}$ obeys Gaussian statistics with the mean and variance*

$$\mathbb{E}(\sigma_1^{(n)}) = \sigma_0 + (\sigma_{\mathrm{c}}^s)^2\sigma_0^{-1}, \qquad \mathrm{Var}\big(\sigma_1^{(n)}\big) = \frac{1}{n}(\sigma_{\mathrm{c}}^s)^2\big(1 - (\sigma_{\mathrm{c}}^s)^2\sigma_0^{-2}\big).$$

c) *For any σ_c^s the second singular value $\sigma_2^{(n)}$ is equal to $2\sigma_{\mathrm{c}}^s$ up to a random correction that is of the order of $n^{-2/3}$ as $n \to \infty$.*

We can describe the ratio of the maximal singular value over the L^2-norm of the other singular values by:

PROPOSITION 4.8. *Let us consider the symmetrized response matrix obtained in the presence of electronic noise with a crack. For $\sigma_{\mathrm{c}}^s < \sigma_0$, the ratio (4.7) has the following statistical distribution*

$$R \overset{dist.}{=} \frac{\sigma_0}{\sigma_{\mathrm{c}}^s} + \frac{\sigma_{\mathrm{c}}^s}{\sigma_0} + \frac{1}{\sqrt{n}}\sqrt{1 - (\sigma_{\mathrm{c}}^s)^2\sigma_0^{-2}}\,\mathcal{N}(0,1). \tag{4.12}$$

For $\sigma_{\mathrm{c}}^s > \sigma_0$ we have (4.11).

4.5. Berens' Modelling Revisited. In [11] A.P. Berens introduced a framework for analyzing schemes for nondestructive inspection methods (NDI), testing for the presence of flaws. In their reliability analysis the probability of detection (POD) as function of flaw size played a central role. In our notation the "flaw size" corresponds to the parameter ε and we are thus interested in designing reliability tests with a desirable performance in terms of the corresponding POD(ε) function. In [11] a maximum likelihood approach was used for parameter estimation, and a log normal distribution was in particular postulated for the response variable's relation to crack size. One parameter to be estimated is then the variance of the Gaussian residual. Our approach here is to introduce a physical model for the measurements, as we have described above, and then infer a corresponding "optimal" POD function that can be associated with the MSR matrix measurements. We describe the picture deriving from this approach below, in fact, the resulting picture deviates somewhat from that deriving from Berens' modelling.

Consider the imaging of cracks from measurements of the MSR matrix at a single frequency ω in the presence of electronic noise, that is, we model with an additive Gaussian noise. Assuming availability of previous and/or multiple measurements we may assume that the variance of the entries of the MSR matrix (due to the electronic noise) is known and equal to a^2. In fact, we will see that we do not need to know the value a^2 in order to build the most powerful test with a prescribed false alarm rate.

By Proposition 4.6, in the absence of the crack (hypothesis H_0) the ratio of the first singular value of the symmetrized MSR matrix over the L^2-norm of the other singular values

$$R := \frac{\sigma_1}{\left(\frac{1}{n-1}\sum_{j=2}^{n-1}\sigma_j^2\right)^{1/2}} \tag{4.13}$$

is of the form

$$R \overset{dist.}{=} 2 + \frac{1}{2^{2/3}n^{2/3}} Z_1, \tag{4.14}$$

where Z_1 is a random variable following a Tracy-Widom distribution of type 1.

In the presence of a crack at position $\boldsymbol{x}^c$ and with size ε (hypothesis H_A), Proposition 4.8 shows that the ratio is of the form

$$R \overset{dist.}{=} \frac{\sigma_0}{\sigma_{\mathrm{c}}^s} + \frac{\sigma_{\mathrm{c}}^s}{\sigma_0} + \frac{1}{\sqrt{n}}\sqrt{1-(\sigma_{\mathrm{c}}^s)^2\sigma_0^{-2}}\,\mathcal{N}(0,1), \tag{4.15}$$

$$\sigma_0(\boldsymbol{x}^c,\varepsilon) = \frac{c_0\sum_{j=1}^{n}\frac{1}{|\boldsymbol{x}_j-\boldsymbol{x}^c|}}{4\omega\,|\log(\frac{\omega\varepsilon}{2c_0})+\gamma-\log 2-\frac{i}{2}|}, \tag{4.16}$$

$$\sigma_{\mathrm{c}}^s = \sqrt{n/2}\,a. \tag{4.17}$$

This result is correct as long as $\sigma_0 > \sigma_{\mathrm{c}}^s$. When $\sigma_0 < \sigma_{\mathrm{c}}^s$ we have (4.14).

Note that, as functions of the number of sensors n, the singular value σ_0 scales as n, while the noise level σ_{c}^s scales as $\sqrt{n}$. This shows that the detection power increases with the number of sensors.

If the data gives the ratio R, then we propose to use a test of the form $R > r$ for the alarm corresponding to the presence of a crack. By the Neyman-Pearson Lemma the decision rule of accepting H_A if and only if $R > r_\alpha$ maximizes the probability of detection for a given false alarm probability α

$$\alpha = \mathbb{P}(R > r_\alpha | H_0)$$

with the threshold

$$r_\alpha = 2 + \frac{1}{2^{2/3}n^{2/3}}\Phi_{\mathrm{TW1}}^{-1}(1-\alpha),$$

where Φ_{TW1} is the cumulative distribution function of the Tracy-Widom distribution of type 1. The computation of the threshold is easy since it depends only on the number of sensors n and on the false alarm probability α. This test is therefore universal. Note that we should use a Tracy-Widom distribution table, and not a Gaussian table. We have, for instance, $\Phi^{-1}_{\mathrm{TW1}}(0.9) \simeq 0.45$, $\Phi^{-1}_{\mathrm{TW1}}(0.95) \simeq 0.98$ and $\Phi^{-1}_{\mathrm{TW1}}(0.99) \simeq 2.02$.

The detection probability $1-\beta$ is the probability to sound the alarm when there is a crack:

$$1-\beta = \mathbb{P}(R > r_\alpha | H_A).$$

For a given measurement array it depends on ε and $\boldsymbol{x}^c$ through the value $\sigma_0(\varepsilon, \boldsymbol{x}^c)$ and also on the noise level a. Here we find that the detection probability is

$$\mathrm{POD}(\varepsilon, \boldsymbol{x}^c) = 1-\beta(\varepsilon, \boldsymbol{x}^c) = 1 - \Phi\left(\sqrt{n}\frac{r_\alpha - \frac{\sigma_0}{\sigma_{\mathrm{c}}^s} - \frac{\sigma_{\mathrm{c}}^s}{\sigma_0}}{\sqrt{1-(\sigma_{\mathrm{c}}^s/\sigma_0)^2}}\right),$$

where Φ is the cumulative distribution function of the normal distribution with mean zero and variance one. This result is valid as long as $\sigma_0 > \sigma_{\mathrm{c}}^s$. When $\sigma_0 < \sigma_{\mathrm{c}}^s$, so that the crack is "hidden in noise", then we have $1-\beta = 1 - \Phi_{\mathrm{TW1}}\big(\Phi^{-1}_{\mathrm{TW1}}(1-\alpha)\big) = \alpha$.

4.6. Rank Estimation of a Noisy Response Matrix. The results of the previous subsections give the principle of an original method to estimate the effective rank of noisy response matrix $\mathbf{A}$ from its singular values $\sigma_1^{(n)} \geq \sigma_2^{(n)} \geq \sigma_3^{(n)} \geq \cdots \geq \sigma_n^{(n)}$. The effective rank of the matrix is the number of non-zero singular values that would be observed in the absence of noise.

The usual procedure consists in estimating the number of singular values larger than a threshold value related to the noise level and determined empirically by the user. The information carried by the small singular values is then not exploited.

Here we propose to look first at the $n-k$ smallest singular values $\sigma_{k+1}^{(n)} \geq \sigma_{k+2}^{(n)} \geq \cdots \geq \sigma_n^{(n)}$, where $k \ll n$ is an upper bound for the effective rank of $\mathbf{A}$. The spectral measure of the $n-k$ smallest singular values is fitted (by a least-square method for instance) by a semi-circle law (note that there is only one parameter to estimate). Then one compares the full histogram of the n singular values with the fitted semi-circle law. The number of singular values that depart significantly from the semi-circle law is the effective rank of the matrix $\mathbf{A}$. A full statistical analysis of this method is possible and will be addressed in a separate paper. Moreover, we will generalize the optimal detection analysis in Section 4 to the case of inclusions and multiple cracks where the matrix $\mathbf{A}$ has more than one significant eigenvalue. This generalization is nontrivial.

5. Conditional Localization. We assume that the spectral test described in Subsection 4.5 identified the presence of a defect and we want to estimate its location. Thus, we want to decide whether there is a defect or not at a particular location based on the measured MSR matrix, $\mathbf{A}$, at a single or for multiple frequencies.

5.1. Effective Imaging Functional. We assume here a single defect, one frequency, and the following model for the noisy MSR matrix:

$$\mathbf{A}(\omega) = \mathbf{A}_0(\omega) + \mathbf{W}(\omega),$$

where $\mathbf{A}_0(\omega)$ is given by (2.4) or (2.6) and $\mathbf{W}$ is a complex centered Gaussian noise with "variance" a^2: $\mathbf{W} = \mathbf{W}_r + i\mathbf{W}_i$, with $\mathbf{W}_r$ and $\mathbf{W}_i$ having identically independently distributed real entries distributed according to the normal distribution with mean 0 and variance $a^2/2$. In particular $\mathbb{E}(|W_{jl}|^2) = a^2$.

Since we know that the unperturbed response matrix $\mathbf{A}_0(\omega)$ is symmetric, we first symmetrize the noisy MSR matrix:

$$\mathbf{A}^s(\omega) = \frac{1}{2}\big(\mathbf{A}(\omega) + \mathbf{A}(\omega)^T\big)$$

which, as said earlier, reduces the noise variance of the off-diagonal entries by a factor of $\sqrt{2}$:

$$\mathbf{A}^s(\omega) = \mathbf{A}_0(\omega) + \mathbf{W}^s(\omega), \qquad \mathbf{W}^s(\omega) = \frac{1}{2}\big(\mathbf{W}(\omega) + \mathbf{W}(\omega)^T\big)$$

Here $\mathbf{W}$ is a symmetric complex Gaussian matrix: $\mathbf{W}^s = \mathbf{W}^s_r + i\mathbf{W}^s_i$, with $\mathbf{W}^s_r$ and $\mathbf{W}^s_i$ being symmetric real matrices with independent entries with mean zero and variance a^2 on the diagonal and $a^2/2$ off the diagonal.

We consider the localization of a crack. We shall first assume that there is one crack present as determined by the spectral detection test described above. Thus, the observations are modelled as

$$\mathbf{A}^s(\omega) = \tau(\omega, \boldsymbol{x})\, \boldsymbol{d}(\omega, \boldsymbol{x})\boldsymbol{d}(\omega, \boldsymbol{x})^T + \mathbf{W}^s(\omega),$$

and we seek to estimate the location $\boldsymbol{x}$ of the crack. Here $\tau, \boldsymbol{d}$ are given by (3.2)-(3.3). In this case, given the parameters $\boldsymbol{x}$, τ, and a, the observed symmetrized response matrix $\mathbf{A}^s(\omega)$ has the probability density function

$$p\left(\mathbf{A}^s \mid \boldsymbol{x}, \tau, a\right) = \frac{1}{2^n \pi^{(n^2+n)/2} a^{n^2+n}} \exp\left(-\frac{\|\mathbf{A}^s - \tau \boldsymbol{d}(\omega, \boldsymbol{x})\boldsymbol{d}(\omega, \boldsymbol{x})^T\|_F^2}{2a^2}\right),$$

with respect to the measure over the space of complex symmetric matrices:

$$\prod_{j=1}^{n} d\Re(A^s_{j,j}) d\Im(A^s_{j,j}) \prod_{1 \le j < l \le n} d\Re(A^s_{j,l}) d\Im(A^s_{j,l}).$$

Here the subscript F represents the Frobenius norm. Using Bayes theorem with the Jeffreys prior for the parameters $\boldsymbol{x}, \tau, a$ (a non-informative prior distribution), which is proportional to a^{-1}, we find that, given the observations $\mathbf{A}^s$, the likelihood function of the parameters $\boldsymbol{x}$, τ, and a is given by:

$$l_0\left(\boldsymbol{x}, \tau, a \mid \mathbf{A}^s\right) = \frac{1}{a^{n^2+n+1}} \exp\left(-\frac{\|\mathbf{A}^s - \tau \boldsymbol{d}(\omega, \boldsymbol{x})\boldsymbol{d}(\omega, \boldsymbol{x})^T\|_F^2}{2a^2}\right). \tag{5.1}$$

The maximum likelihood estimator of $\boldsymbol{x}$ and the nuisance parameters a and τ are found by maximizing the likelihood function (5.1) with respect to these:

$$\big(\hat{\boldsymbol{x}}, \hat{\tau}, \hat{a}\big) = \arg\max_{\boldsymbol{x}, \tau, a} l_0\left(\boldsymbol{x}, \tau, a \mid \mathbf{A}^s\right).$$

We first eliminate a by requiring

$$\left.\frac{\partial l_0\left(\boldsymbol{x}, \tau, a \mid \mathbf{A}^s\right)}{\partial a}\right|_{a=\hat{a}} = 0,$$

which gives

$$\hat{a} = \frac{\|\mathbf{A}^s - \tau \boldsymbol{d}(\omega, \boldsymbol{x})\boldsymbol{d}(\omega, \boldsymbol{x})^T\|_F}{\sqrt{n^2+n+1}},$$

and then the likelihood ratio is proportional to

$$l_0\big(\boldsymbol{x}, \tau, \hat{a} \mid \mathbf{A}^s\big) \simeq \|\mathbf{A}^s - \tau \boldsymbol{d}(\omega, \boldsymbol{x})\boldsymbol{d}(\omega, \boldsymbol{x})^T\|_F^{-(n^2+n+1)/2}.$$

Since $\mathbf{A}^s(\omega)$ is complex symmetric, it admits a symmetric singular value decomposition: there exist unitary vectors $\boldsymbol{u}_j(\omega)$ and nonnegative numbers $\sigma_j(\omega)$ (the singular values) such that

$$\mathbf{A}^s(\omega) = \sum_{j=1}^{n} \sigma_j(\omega) \boldsymbol{u}_j(\omega) \boldsymbol{u}_j(\omega)^T.$$

Therefore, we can write

$$\|\mathbf{A}^s - \tau \boldsymbol{d}(\omega, \boldsymbol{x}) \boldsymbol{d}(\omega, \boldsymbol{x})^T\|_F^2 = \|\boldsymbol{u}^{(2)}(\omega) - \tau \boldsymbol{d}^{(2)}(\omega, \boldsymbol{x})\|_2^2,$$

with $\boldsymbol{u}^{(2)} = \sum_{j=1}^{n} \sigma_j \boldsymbol{u}_j \otimes \boldsymbol{u}_j$ and $\boldsymbol{d}^{(2)} = \boldsymbol{d} \otimes \boldsymbol{d}$. Since $\|\boldsymbol{d}\| = 1$, we have $\|\boldsymbol{d}^{(2)}\|_2 = 1$ and we then find that

$$\hat{\tau} = \arg\min_{\tau} \|\boldsymbol{u}^{(2)}(\omega) - \tau \boldsymbol{d}^{(2)}(\omega, \boldsymbol{x})\|_2^2 = \big(\boldsymbol{d}^{(2)}(\omega, \boldsymbol{x}), \boldsymbol{u}^{(2)}(\omega)\big).$$

Note also that $\|\boldsymbol{u}^{(2)}\|_2^2 = \sum_{j=1}^{n} \sigma_j^2 = \|\mathbf{A}^s\|_F^2$. We therefore conclude that the maximum likelihood estimator $\hat{\boldsymbol{x}}$ derives from maximizing the MUSIC-type function

$$\hat{\boldsymbol{x}} = \arg\min_{\boldsymbol{x}} \big\|\boldsymbol{u}^{(2)}(\omega) - \big(\boldsymbol{d}^{(2)}(\omega, \boldsymbol{x}), \boldsymbol{u}^{(2)}(\omega)\big) \boldsymbol{d}^{(2)}(\omega, \boldsymbol{x})\big\|_2^2.$$

Note however that $\hat{\boldsymbol{x}}$ is not the maximizer of the MUSIC functional (3.5) since all singular vectors (weighted by the singular values) contribute to $\boldsymbol{u}^{(2)}$. We have in fact

$$\begin{aligned} \big\|\boldsymbol{u}^{(2)}(\omega) - \big(\boldsymbol{d}^{(2)}(\omega, \boldsymbol{x}), \boldsymbol{u}^{(2)}(\omega)\big) \boldsymbol{d}^{(2)}(\omega, \boldsymbol{x})\big\|_2^2 &= \|\boldsymbol{u}^{(2)}(\omega)\|_2^2 - \big|(\boldsymbol{u}^{(2)}(\omega), \boldsymbol{d}^{(2)}(\omega, \boldsymbol{x}))\big|^2 \\ &= \|\mathbf{A}^s(\omega)\|_F^2 - |\mathcal{I}_{\mathrm{KM}}(\omega, \boldsymbol{x})|^2, \end{aligned}$$

where $\mathcal{I}_{KM}$ is the Kirchhoff migration functional (3.6). From this representation we find that the estimation $\hat{\boldsymbol{x}}$ of the location can be expressed in terms of the Kirchhoff migration functional as

$$\hat{\boldsymbol{x}} = \arg\max_{\boldsymbol{x}} |\mathcal{I}_{\mathrm{KM}}(\omega, \boldsymbol{x})|. \tag{5.2}$$

This indicates that Kirchhoff migration is more accurate in the presence of additive noise than MUSIC in that the location of its maximum is exactly the maximum likelihood estimator of the location of the crack.

The analysis can be extended to the case in which the response matrices are recorded at several frequencies $(\omega_k)_{k=1,\dots,K}$ and the additive noise matrices $\mathbf{W}(\omega_k)$, $k = 1, \dots, K$, are independent and identically distributed. Then one finds that the maximum likelihood estimator of the location of the defect is the maximum of the matched field imaging functional:

$$\hat{\boldsymbol{x}} = \arg\max_{\boldsymbol{x}} \mathcal{I}_{\mathrm{MF}}(\boldsymbol{x}), \tag{5.3}$$

where $\mathcal{I}_{MF}$ is the Matched Field functional (3.11). This shows that one should look for the maximum of the sum of the square moduli of the KM functionals in order to exploit the multi-frequency information optimally. Indeed, the fact that the relevant operation is the sum of the squares comes from the fact that the additive noise matrices are assumed to be independent for different frequencies. If some correlation between frequency components exists, it is likely that a procedure such as Coherent Interferometry [12] will be more appropriate.

5.2. Multiple Localization via Projection Pursuit. We remark here on the case when there are several cracks. We can then use a recursively applied and projected version of the approach above. Let $\Pi_k^\perp$ denote the unitary projection matrix on the complement of the subspace spanned by the illuminated vectors $\boldsymbol{d}(\omega, \hat{\boldsymbol{x}}_j), j = 1, .., k$ of the first k estimated crack locations.

We then form the modified MSR matrix by projecting as:

$$\mathbf{A}_k^s(\omega) = \Pi_k^\perp \mathbf{A}^s(\omega) \Pi_k^\perp. \tag{5.4}$$

The test for presence of further cracks is then carried out as described in Section 4.5, but with respect to the projected MSR. In the case that the test predicts that further cracks are present then the subsequent crack location is estimated by again maximizing a Kirchhoff imaging functional $\mathcal{I}_{\mathrm{KM},k}$, associated with the projected MSR $\mathbf{A}_k^s$.

We remark that above we assumed that the cracks were well-separated so that the corresponding illumination vectors are orthogonal. In the case that clusters of nearby cracks are present one can generalize the above approach by postprocessing the data such that the location estimates for the cracks in the cluster is estimated by maximizing the joint likelihood of the cracks.

5.3. Statistical Analysis of Location Estimate. We continue here the analysis of the single frequency case and provide a location-dependent threshold for the image function that we derived above. We remark that this is important since the detection test introduced in Section 4 tests whether there is something present in the probed scenery or not. Here we want to test whether there is a localized crack present at the particular search location $\boldsymbol{x}^S$. As a part of this test we will then obtain a measure of confidence with which we can say that there is a crack present.

We choose as a test statistics the image function derived above

$$\mathcal{I}_{\mathrm{KM}}(\omega, \boldsymbol{x}^S) = \big(\boldsymbol{d}(\omega, \boldsymbol{x}^S), \mathbf{A}^s(\omega)\overline{\boldsymbol{d}(\omega, \boldsymbol{x}^S)}\big) = \big(\boldsymbol{d}(\omega, \boldsymbol{x}^S), \mathbf{A}(\omega)\overline{\boldsymbol{d}(\omega, \boldsymbol{x}^S)}\big).$$

We observe that under the null hypothesis H_0, there is no crack at $\boldsymbol{x}^S$, we have

$$\mathcal{I}_{\mathrm{KM}}(\omega, \boldsymbol{x}^S) \overset{dist.}{\simeq} \frac{a}{\sqrt{2}}(W_1 + iW_2),$$

with W_j being standard independent normal real Gaussian random variables with mean zero and variance one. Here a^2 is the variance of the entries of the random matrix $\mathbf{A}$ and we have implicitly assumed that $\boldsymbol{x}^S$ is far enough from the other cracks so that the vector $\boldsymbol{d}(\omega, \boldsymbol{x}^S)$ is approximately orthogonal to the illumination vectors of other cracks. Under the alternate hypothesis H_A, we have

$$\mathcal{I}_{\mathrm{KM}}(\omega, \boldsymbol{x}^S) \overset{dist.}{\simeq} \mu_{\mathrm{KM}}(\omega, \boldsymbol{x}^S) + \frac{a}{\sqrt{2}}(W_1 + iW_2),$$

where $\mu_{\mathrm{KM}}(\omega, \boldsymbol{x}^S)$ is given by

$$\mu_{\mathrm{KM}}(\omega, \boldsymbol{x}^S) = \tau(\omega, \boldsymbol{x}^S)\big|\boldsymbol{d}(\omega, \boldsymbol{x}^S)\big|^4 = \tau(\omega, \boldsymbol{x}^S),$$

with τ given by (3.3).

We now consider the real and imaginary parts of the statistics:

$$y_1 = \Re(\mathcal{I}_{\mathrm{KM}}(\omega, \boldsymbol{x}^S)), \qquad y_2 = \Im(\mathcal{I}_{\mathrm{KM}}(\omega, \boldsymbol{x}^S)).$$

and we denote similarly $\mu_1 = \Re(\mu_{\mathrm{KM}}(\omega, \boldsymbol{x}^S))$ and $\mu_2 = \Im(\mu_{\mathrm{KM}}(\omega, \boldsymbol{x}^S))$. From the expression (3.3) of $\tau(\omega, \boldsymbol{x}^S)$, it is clear that its argument is very close to $\pi/2$ so that

μ_2 is positive and larger than μ_1 and the relevant information is in the imaginary part of the imaging functional $y_2 = \Im(\mathcal{I}_{\rm KM}(\omega, \boldsymbol{x}^S))$. Using the expression of the normal density we find that the likelihood ratio for y_2 is given by

$$\Lambda(y_2) = \frac{f_A(y_2)}{f_0(y_2)} = \exp\Big(- \frac{\mu_2^2}{a^2} + \frac{2\mu_2 y_2}{a^2}\Big).$$

By the Neyman-Pearson Lemma the decision rule of accepting H_A if and only if $y_2 = \Im(\mathcal{I}_{\rm KM}(\omega, \boldsymbol{x}^S)) > \eta$ maximizes the probability of detection for a given false alarm rate α with the threshold $\eta = (a/\sqrt{2})\Phi^{-1}(1-\alpha)$, where Φ is the cumulative distribution function of the normal distribution. The power of the test is given by

$$1 - \beta_{\rm KM}(\omega, \boldsymbol{x}^S) = 1 - \Phi\Big(\sqrt{2}\frac{\eta - \Im(\mu_{\rm KM}(\omega, \boldsymbol{x}^S))}{a}\Big) = \Phi\Big(\sqrt{2}\frac{\Im(\mu_{\rm KM}(\omega, \boldsymbol{x}^S)) - \eta}{a}\Big), \tag{5.5}$$

since $\Phi(\boldsymbol{x}) = 1 - \Phi(-\boldsymbol{x})$.

The power of the test can be expressed in terms of the SNR

$$\mathrm{SNR}(\omega, \boldsymbol{x}^S) = \frac{\big|\mathbb{E}\big(\mathcal{I}_{\rm KM}(\omega, \boldsymbol{x}^S)\big)\big|}{\mathrm{Var}^{1/2}\big(\mathcal{I}_{\rm KM}(\omega, \boldsymbol{x}^S)\big)} = \frac{|\tau(\omega, \boldsymbol{x}^S)|}{a},$$

as

$$1 - \beta_{\rm KM}(\omega, \boldsymbol{x}^S) = \Phi\Big(\sqrt{2}\mathrm{SNR}(\omega, \boldsymbol{x}^S) - \Phi^{-1}(1-\alpha)\Big), \tag{5.6}$$

where we have made the approximation $|\mu_{\rm KM}(\omega, \boldsymbol{x}^S)| \simeq \Im(\mu_{\rm KM}(\omega, \boldsymbol{x}^S))$ which is accurate enough since the argument of $\tau(\omega, \boldsymbol{x}^S)$ is close to $\pi/2$. Note that the order of magnitude of the SNR is

$$\mathrm{SNR}(\omega_0, \boldsymbol{x}^S) \simeq \mathrm{SNR}_0 := \frac{c_0 n}{4\omega_0 L\Big|\log(\frac{\omega_0 \varepsilon}{2c_0}) + \gamma - \log 2 - \frac{i}{2}\Big|}, \tag{5.7}$$

where ω_0 is the typical frequency and L is the distance from the sensor array to the search region.

5.4. Multifrequency Measurements. In the case of (uncorrelated) measurements at multiple frequencies, one can use the migration imaging functional (3.9) which can be written as

$$\mathcal{I}_{\rm KMF}(\boldsymbol{x}^S) = \frac{1}{K}\sum_{\omega_k} \mathcal{I}_{\rm KM}(\omega_k, \boldsymbol{x}^S),$$

where K is the number of frequencies. Under the null hypothesis H_0, there is no defect at $\boldsymbol{x}^S$, the functional $\mathcal{I}_{\rm KMF}(\boldsymbol{x}^S)$ is distributed as

$$\mathcal{I}_{\rm KMF}(\boldsymbol{x}^S) \overset{dist.}{\simeq} \frac{a}{\sqrt{2K}}(W_1 + iW_2)$$

with again W_j being standard independent normal real Gaussian random variables with mean zero and variance one. Under the alternate hypothesis H_A, we have

$$\mathcal{I}_{\rm KMF}(\boldsymbol{x}^S) \overset{dist.}{\simeq} \mu_{\rm KMF}(\boldsymbol{x}^S) + \frac{a}{\sqrt{2K}}(W_1 + iW_2),$$

where $\mu_{\rm KMF}(\boldsymbol{x}^S)$ is given by

$$\mu_{\rm KMF}(\boldsymbol{x}^S) = \frac{1}{K}\sum_{\omega_k} \mu_{\rm KM}(\omega_k, \boldsymbol{x}^S).$$

A straightforward generalization of the arguments used in the previous subsection shows that the test accepting H_A if $\Im(\mathcal{I}_{\rm KMF}(\boldsymbol{x}^S)) > \eta$ maximizes the probability of detection for a given false alarm rate α with the threshold $\eta = (a/\sqrt{2K})\Phi^{-1}(1-\alpha)$. The power of this test is

$$\begin{aligned} 1 - \beta_{\rm KMF}(\boldsymbol{x}^S) &= \Phi\Big(\sqrt{2K}\frac{\Im(\mu_{\rm KMF}(\boldsymbol{x}^S)) - \eta}{a}\Big) \\ &\simeq \Phi\Big(\sqrt{2K}\ {\rm SNR}_0 - \Phi^{-1}(1-\alpha)\Big), \end{aligned} \tag{5.8}$$

with ${\rm SNR}_0$ defined by (5.7). Therefore, the multiple frequencies enhance the detection performance via higher "effective" SNR.

One can also use the matched field imaging functional (3.11)

$$\mathcal{I}_{\rm MF}(\boldsymbol{x}^S) = \frac{1}{K}\sum_{\omega_k} |\mathcal{I}_{\rm KM}(\omega_k, \boldsymbol{x}^S)|^2.$$

Under the null hypothesis H_0, there is no defect at $\boldsymbol{x}^S$, the distribution of the functional $\mathcal{I}_{\rm MF}(\boldsymbol{x}^S)$ is proportional to a χ^2-distribution with $2K$ degrees of freedom and it can be approximated when K is large enough ($2K > 50$ in practice) by

$$\mathcal{I}_{\rm MF}(\boldsymbol{x}^S) \overset{dist.}{\simeq} a^2 + \frac{a^2}{\sqrt{K}}\mathcal{N}(0,1).$$

Under the alternate hypothesis H_A, we have for K large enough

$$\mathcal{I}_{\rm MF}(\boldsymbol{x}^S) \overset{dist.}{\simeq} a^2 + \mu^2_{\rm MF}(\boldsymbol{x}^S) + \frac{a}{\sqrt{K}}\sqrt{2\mu^2_{\rm MF}(\boldsymbol{x}^S) + a^2}\mathcal{N}(0,1),$$

where $\mu_{\rm MF}(\boldsymbol{x}^S)$ is given by

$$\mu^2_{\rm MF}(\boldsymbol{x}^S) = \frac{1}{K}\sum_{\omega_k} |\mu_{\rm KM}(\omega_k, \boldsymbol{x}^S)|^2 = \frac{1}{K}\sum_{\omega_k} |\tau(\omega_k, \boldsymbol{x}^S)|^2.$$

The test accepting H_A if $\mathcal{I}_{\rm MF}(\boldsymbol{x}^S) > \eta$ maximizes the probability of detection for a given false alarm rate α with the threshold

$$\eta = a^2 + \frac{a^2}{\sqrt{K}}\Phi^{-1}(1-\alpha).$$

The power of this test is

$$1 - \beta_{\rm MF}(\boldsymbol{x}^S) = \Phi\Big(\sqrt{K}\frac{\mu^2_{\rm MF}(\boldsymbol{x}^S)}{a\sqrt{a^2 + 2\mu^2_{\rm MF}(\boldsymbol{x}^S)}} - \frac{a}{\sqrt{a^2 + 2\mu^2_{\rm MF}(\boldsymbol{x}^S)}}\Phi^{-1}(1-\alpha)\Big),$$

If the SNR is larger than one, then the power is

$$1 - \beta_{\rm MF}(\boldsymbol{x}^S) = \Phi\Big(\frac{\sqrt{K}}{\sqrt{2}}{\rm SNR}_0 - {\rm SNR}_0^{-1}\Phi^{-1}(1-\alpha)\Big).$$

If the SNR is smaller than one, then the power is

$$1 - \beta_{\rm MF}(\boldsymbol{x}^S) = \Phi\Big(\sqrt{K}{\rm SNR}_0^2 - \Phi^{-1}(1-\alpha)\Big).$$

This shows that the power is smaller than with the test using the KMF functional.

6. Resolution Analysis. Following [19], we provide a resolution analysis for imaging or localization of defects in the presence of noise. We do this in the context of a small inclusion.

Suppose that there are two inclusions $D_s = \varepsilon B_s + \boldsymbol{x}_s^c, s = 1, 2$ with permeabilities μ_s and the same permittivity as the background $q = 1$. If the inclusions are well separated then the leading-order term in the asymptotic expansion of the MSR matrix (as $\omega \to +\infty$ and $\varepsilon\omega \to 0$) is the sum of the two inclusion contributions:

$$A_{jl}(\omega) = \varepsilon^2 \sum_{s=1}^{2} \nabla\hat{G}(\omega, \boldsymbol{x}_j, \boldsymbol{x}_s^c) \cdot \mathbf{M}(\mu_s, B_s) \nabla\hat{G}(\omega, \boldsymbol{x}_s^c, \boldsymbol{x}_l) + \mathrm{o}\Big(\frac{\varepsilon^2\omega^2}{c_0^2}\Big), \quad (6.1)$$

while if the inclusions are closely spaced then we have [7]:

$$A_{jl}(\omega) = \varepsilon^2 \nabla\hat{G}(\omega, \boldsymbol{x}_j, \overline{\boldsymbol{x}^c}) \cdot \mathbf{M}(\overline{\mu}, \overline{B}) \nabla\hat{G}(\omega, \overline{\boldsymbol{x}^c}, \boldsymbol{x}_l) + \mathrm{o}\Big(\frac{\varepsilon^2\omega^2}{c_0^2}\Big), \quad (6.2)$$

where $\overline{B}$ is an equivalent ellipse with the overall $\overline{\mu}$ and of center $\overline{\boldsymbol{x}^c}$ given by

$$\frac{1-\overline{\mu}}{1+\overline{\mu}} \sum_{s=1}^{2} |B_s| = \sum_{s=1}^{2} \frac{1-\mu_s}{1+\mu_s} |B_s|,$$

and

$$\frac{1-\overline{\mu}}{1+\overline{\mu}} \overline{\boldsymbol{x}^c} \sum_{s=1}^{2} |B_s| = \sum_{s=1}^{2} \frac{1-\mu_s}{1+\mu_s} |B_s| \boldsymbol{x}_s^c.$$

Formula (6.2) says that the signature of the two inclusions is the same as an equivalent one placed at the location $\overline{\boldsymbol{x}^c}$ and with the permeability $\overline{\mu}$.

Consider now an imaging functional $\mathcal{I}(\boldsymbol{x}^S)$ of the same form as before (for instance (3.14) where the contributions of the two inclusions are renormalized). In the presence of noise, we decide between two alternatives:

- H_0: there is one defect,
- H_A: there are two defects.

We assume here that the distribution of the imaging functional is Gaussian. We use $\mathcal{I}(\overline{\boldsymbol{x}^c})$ as the basis for our decision. Under the null hypothesis we have $\mathcal{I}(\overline{\boldsymbol{x}^c}) \sim \mathcal{N}(\mu_1, \delta)$ while under the alternative hypothesis $\mathcal{I}(\overline{\boldsymbol{x}^c}) \sim \mathcal{N}(\mu_2, \delta)$, where the means μ_1 and μ_2 can be computed explicitly. The mean μ_2 depends on the distance ρ between the centers of the inclusions.

Let α denote the false alarm rate. The decision rule is to accept H_A when $\mathcal{I}(\overline{\boldsymbol{x}^c})$ goes below a certain threshold η determined by

$$\eta = \mu_1 + \delta\Phi^{-1}(\alpha),$$

which is independent of ρ. The detection probability for a two-defects is then given by

$$1 - \beta(\rho) = \Phi\left(\frac{\eta - \mu_2(\rho)}{\delta}\right) = \Phi\left(\Phi^{-1}(\alpha) + \frac{\mu_1 - \mu_2(\rho)}{\delta}\right).$$

According to the Neyman-Person Lemma, the detector is the most powerful in the sense that it produces the highest detection probability for all values of the unknown distance ρ and a given false alarm rate α.

One then introduces the following notion of detection resolution, ρ_r: *the offset that gives a* 50% *chance of detecting the presence of two inclusions*, that is,

$$\beta(\rho_r) = \frac{1}{2}.$$

7. Reconstruction of Geometric Features.

7.1. Identification of Crack Orientation. Assume that one has detected a crack at location $\boldsymbol{x}^c$ and seeks to estimate the orientation of the crack. To this effect note that we have from (2.4)

$$\mathcal{A}(j,l,\omega) := \frac{16\omega^2|\boldsymbol{x}_j-\boldsymbol{x}^c||\boldsymbol{x}_l-\boldsymbol{x}^c|}{c_0^2}A_{jl}\overline{A}_{jl} \sim a_0^\varepsilon + \omega^2 a_1^\varepsilon(\boldsymbol{n}_j\cdot\boldsymbol{t})(\boldsymbol{n}_l\cdot\boldsymbol{t}),$$

for

$$a_0^\varepsilon = \frac{1}{|\log(\frac{\omega\varepsilon}{2c_0})+\gamma-\log 2-\frac{i}{2}|^2}, \quad a_1^\varepsilon = -\frac{\varepsilon^2}{c_0^2}\,\Re\Big(\frac{1}{\log(\frac{\omega\varepsilon}{2c_0})+\gamma-\log 2-\frac{i}{2}}\Big),$$

$$\boldsymbol{n}_j = \frac{\boldsymbol{x}^c-\boldsymbol{x}_j}{|\boldsymbol{x}^c-\boldsymbol{x}_j|}.$$

Since a_0^ε and a_1^ε can be estimated from σ_1, the procedure for estimation of $\boldsymbol{t}$ exploits the frequency dependence of $\mathcal{A}(j,l,\omega)$ as follows:

$$\hat{\boldsymbol{t}} = \text{argmin}_{\boldsymbol{t}} \sum_{j,l,\omega_k}\Big|\mathcal{A}(j,l,\omega_k) - \hat{a}_0^\varepsilon - \omega_k^2\hat{a}_1^\varepsilon(\boldsymbol{n}_j\cdot\boldsymbol{t})(\boldsymbol{n}_l\cdot\boldsymbol{t})\Big|^2, \tag{7.1}$$

with the "hats" representing estimates.

7.2. Identification of Polarization Tensor. Assume that one has detected an inclusion at $\boldsymbol{x}^c$ and seeks to estimate its polarization tensor $\varepsilon^2\mathbf{M}(\mu,B)(=\mathbf{M}(\mu,D))$ and $\rho := |D|(q-1)$. In contrast with the crack detection problem, using measurements at multiple frequencies does not yield better reconstruction of the geometric features and material parameters of the inclusion since the leading-order term in A_{jl} depends linearly on the frequency (see (2.6)).

Writing $\mathbf{M}(\mu,D) = \lambda_1\boldsymbol{w}_1\otimes\boldsymbol{w}_1+\lambda_2\boldsymbol{w}_2\otimes\boldsymbol{w}_2$, where $\boldsymbol{w}_1$ and $\boldsymbol{w}_2$ are orthonormal eigenvectors of $\mathbf{M}(\mu,D)$, we have

$$\begin{aligned}\mathcal{A}(j,l,\omega) &:= \frac{64\pi^2c_0^2}{\varepsilon^4\omega^2}|\boldsymbol{x}_j-\boldsymbol{x}^c||\boldsymbol{x}_l-\boldsymbol{x}^c|A_{jl}\overline{A}_{jl}\\ &\simeq \Big[\sum_{m=1}^2\frac{\lambda_m(\boldsymbol{x}_j-\boldsymbol{x}^c)\cdot\boldsymbol{w}_m(\boldsymbol{x}_l-\boldsymbol{x}^c)\cdot\boldsymbol{w}_m}{|\boldsymbol{x}_j-\boldsymbol{x}^c||\boldsymbol{x}_l-\boldsymbol{x}^c|}+|D|(q-1)\Big]^2.\end{aligned} \tag{7.2}$$

Therefore, we obtain that

$$\begin{aligned}&(\hat{\lambda_1},\hat{\boldsymbol{w}}_1,\hat{\lambda_2},\hat{\boldsymbol{w}}_2,\hat{\rho})\\ &= \text{argmin}_{\lambda_1,\boldsymbol{w}_1,\lambda_2,\boldsymbol{w}_2,\rho}\sum_{j,l,\omega_k}\Big|\mathcal{A}(j,l,\omega_k) - \Big[\sum_{m=1}^2\frac{\lambda_m(\boldsymbol{x}_j-\boldsymbol{x}^c)\cdot\boldsymbol{w}_m(\boldsymbol{x}_l-\boldsymbol{x}^c)\cdot\boldsymbol{w}_m}{|\boldsymbol{x}_j-\boldsymbol{x}^c||\boldsymbol{x}_l-\boldsymbol{x}^c|}+\rho\Big]^2\Big|^2,\end{aligned}$$

with the "hats" representing as before estimates.

8. Numerical Experiments. This section presents results of numerical experiments that give qualitative illustrations of some of the main findings in this paper. We choose the following cracks:

$$\begin{aligned}\Sigma_1 &= \{(x+0.2,-11.5) : -\varepsilon\le x\le\varepsilon\},\\ \Sigma_2 &= \{R_{\pi/6}(x-0.4,-10.5) : -\varepsilon\le x\le\varepsilon\},\end{aligned}$$

where $R_{\pi/6}$ is the rotation by $\pi/6$, *i.e.*, $\boldsymbol{t} = \big(\cos\frac{\pi}{6},\sin\frac{\pi}{6}\big)$. We set $\varepsilon = 0.01$ and suppose that the transducers are equidistributed on the line going from $(x_1^{(1)},0)$ to $(x_1^{(N)},0)$.

8.1. Imaging Functionals. First, we consider imaging of a single crack using the functionals $\mathcal{I}_{\mathrm{MU}}$, $\mathcal{I}_{\mathrm{KM}}$, $\mathcal{I}_{\mathrm{KMF}}$, and $\mathcal{I}_{\mathrm{MT}}$ to illustrate their performance and limitations. Recall that these are the "Music", "Kirchhoff", "Multifrequency Kirchhoff" and "One Mode Kirchhoff" given in respectively (3.5), (3.6), (3.9) and (3.10) in the situation with a crack. The test configurations are given in Table 8.1. Note that the set of data is generated by numerically solving the forward problem, that is solving (2.1), using an integral equation code.

Crack	n	$x_1^{(1)}$	$x_1^{(n)}$	Frequency	Imaging functional	Figure
Σ_1	20	-1	1	$\omega \in [300, 360]$	$\mathcal{I}_{MT}, \mathcal{I}_{KMF}, \mathcal{I}_{KM}$	Figs. 8.1, 8.4
Σ_2	20	-1	1	$\omega \in [300, 360]$	$\mathcal{I}_{MT}, \mathcal{I}_{KMF}, \mathcal{I}_{KM}$	Figs. 8.2, 8.5
Σ_1	20	-1	1	$\omega = 330$	$\mathcal{I}_{MU}$	Figs. 8.1, 8.4,8.3
Σ_2	20	-1	1	$\omega = 330$	$\mathcal{I}_{MU}$	Figs. 8.2, 8.5

TABLE 8.1
Test configurations.

The interval $[300, 360]$ is uniformly partitioned into $K = 60$ frequencies. The discretization size of the search domain is chosen as 0.05.

Localization results for Σ_1 and Σ_2 are shown in Figs. 8.1 and 8.2, respectively. The locations of Σ_1 and Σ_2 are successfully identified. However, the location of the rotated crack Σ_2 is not well-identified using $\mathcal{I}_{\mathrm{MU}}$.

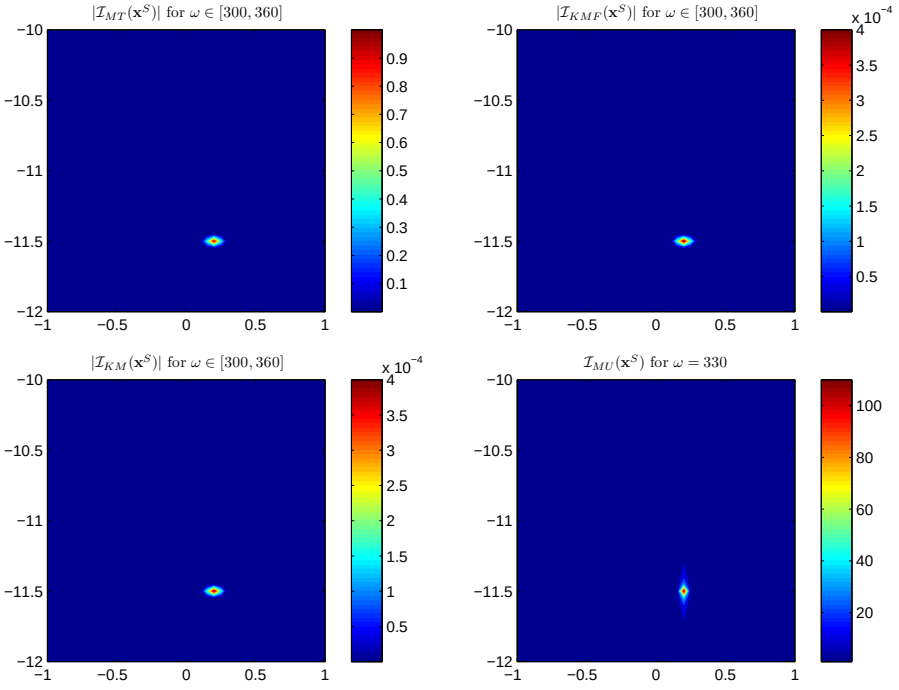

FIG. 8.1. *Localization results for Σ_1 using $\mathcal{I}_{\mathrm{MT}}$ (top left), $\mathcal{I}_{\mathrm{KMF}}$ (top right), $\mathcal{I}_{\mathrm{KM}}$ (bottom left) and $\mathcal{I}_{\mathrm{MU}}$ (bottom right). The data set is generated solving (2.4) numerically.*

Fig. 8.3 shows that the performance of the MUSIC algorithm over the considered range of frequencies $[300, 360]$ is almost invariant. In the the other examples, we shall use the middle frequency, $\omega = 330$, for this single-frequency algorithm.

Let us stress that using data computed by the asymptotic expansion formula (2.4) yields closely resembling images. In Figs. 8.4 and 8.5, localization results for Σ_1 and Σ_2 using the asymptotic expansion formula are shown. That the imaging

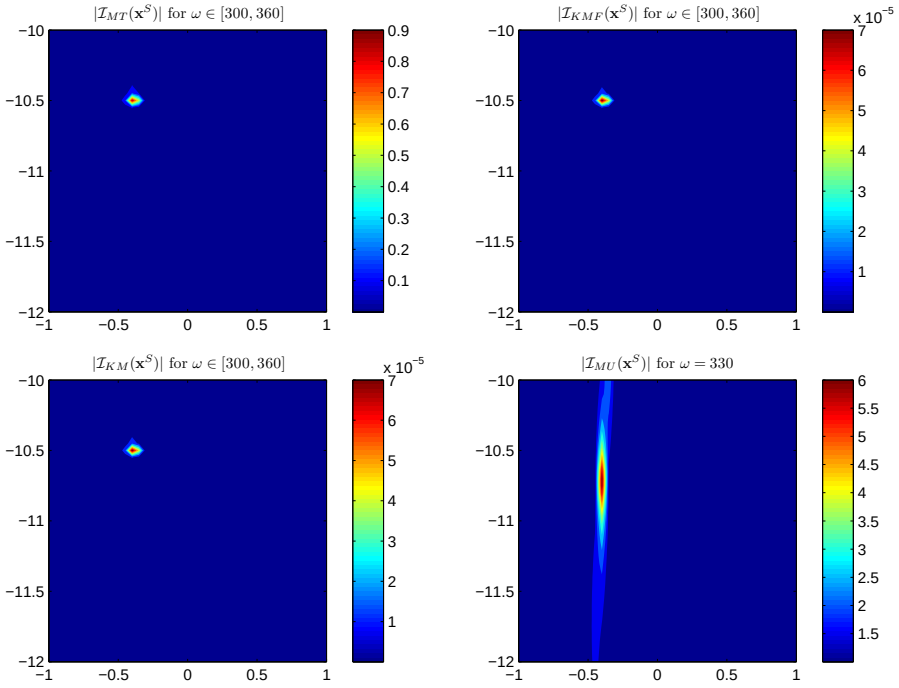

FIG. 8.2. *Localization results for* Σ_2.

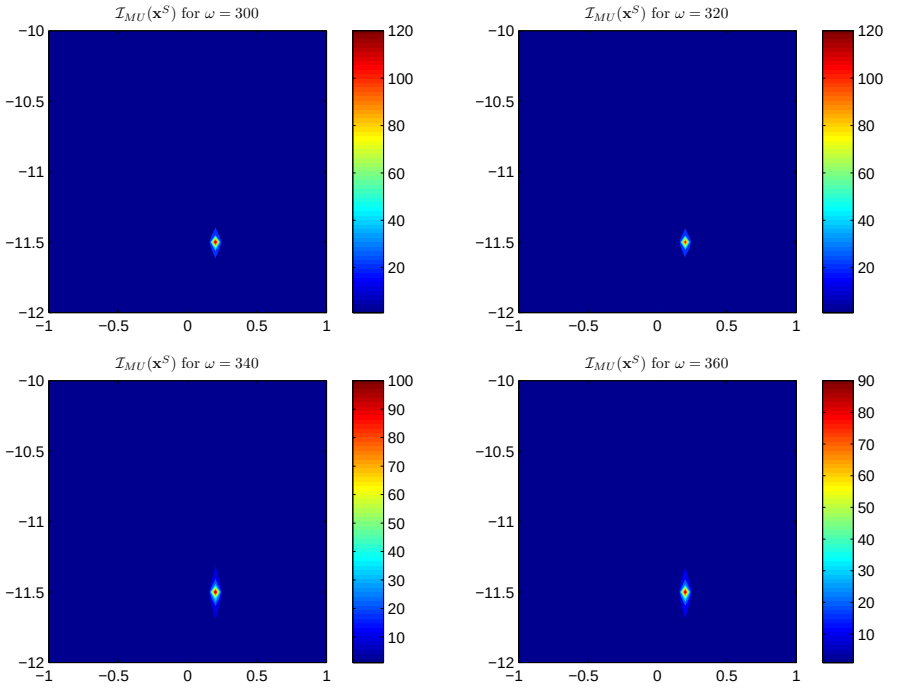

FIG. 8.3. *Localization results for* Σ_1 *using* $\mathcal{I}_{MU}$ *with* $\omega = 300, 320, 340,$ *and* 360.

functionals are efficient when the forward problem is computed with the asymptotic formulas is indeed expected as they have been constructed via this representation. The comparisons between Figs. 8.4-8.5 and Figs. 8.1-8.2, however, show that the imaging functionals are efficient as well when the forward data is generated by

solving (2.1) numerically, giving data which reflects more closely a situation with "real data".

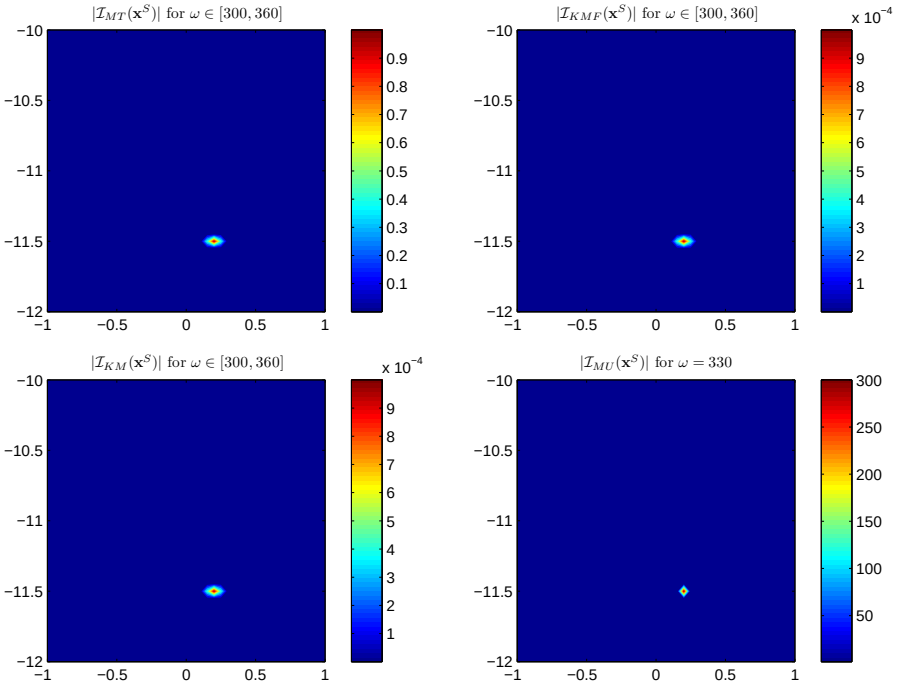

FIG. 8.4. *Localization results for Σ_1 using $\mathcal{I}_{\mathrm{MT}}$ (top left), $\mathcal{I}_{\mathrm{KMF}}$ (top right), $\mathcal{I}_{\mathrm{KM}}$ (bottom left) and $\mathcal{I}_{\mathrm{MU}}$ (bottom right). The data set is generated using the asymptotic formula (2.4).*

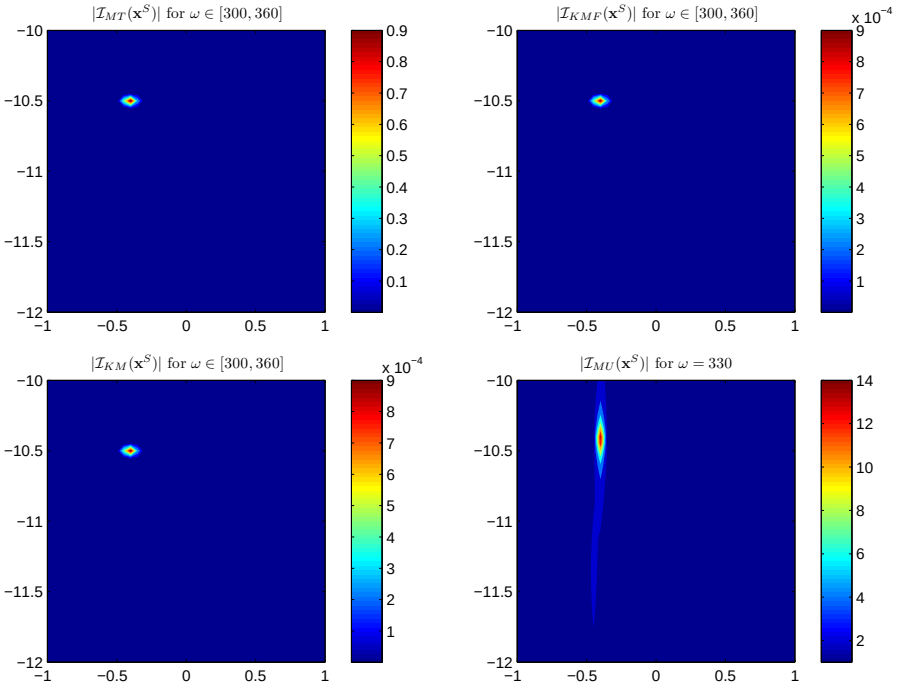

FIG. 8.5. *Same as Fig. 8.4 except that the crack is Σ_2.*

8.1.1. Influence of the Transducer Array Setting. Next, we show the influence of the configuration of the transducer array with the test configurations being described in Table 8.2. The used imaging functional is $\mathcal{I}_{\mathrm{MT}}$.

Crack	n	$x_1^{(1)}$	$x_1^{(n)}$	Frequency	Imaging functional	Setting
Σ_2	20	-0.5	0.5	$\omega \in [300, 360]$	$\mathcal{I}_{\mathrm{MT}}$	setting 1
Σ_2	20	-1	1	$\omega \in [300, 360]$	$\mathcal{I}_{\mathrm{MT}}$	setting 2
Σ_2	20	-2	2	$\omega \in [300, 360]$	$\mathcal{I}_{\mathrm{MT}}$	setting 3
Σ_2	20	-5	5	$\omega \in [300, 360]$	$\mathcal{I}_{\mathrm{MT}}$	setting 4

TABLE 8.2
Test configuration.

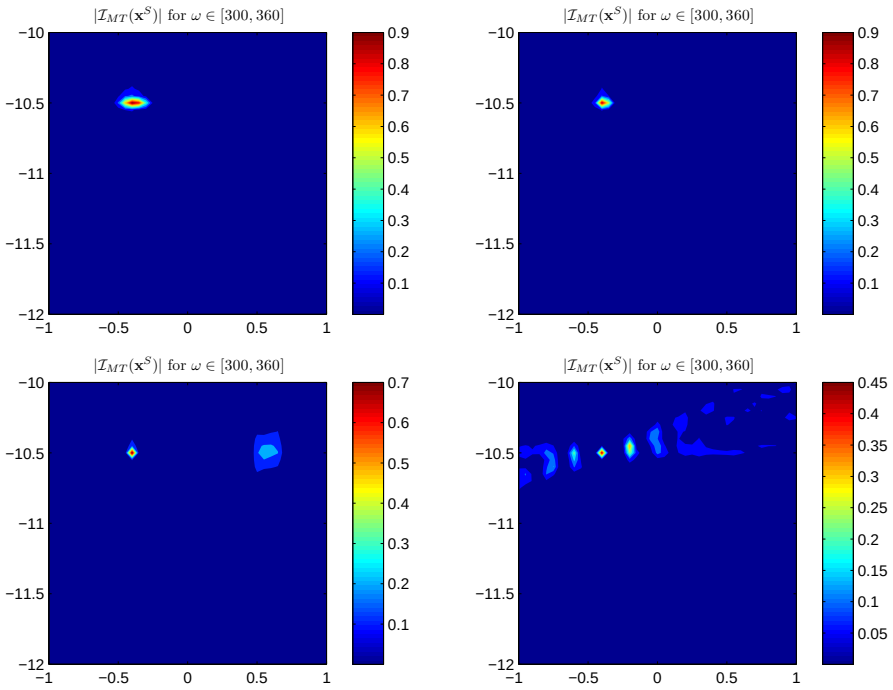

FIG. 8.6. *Results for Σ_2. Top left: setting 1, top right: setting 2, bottom left: setting 3 and bottom right: setting 4.*

In Fig. 8.6, we can see that for a given number of transducers, if the size of the array is small then the images are blurred while if it is large, then an aliasing effect due to undersampling of the array can appear.

8.1.2. Estimation of the Tangential Direction of a Crack. We now estimate the tangential direction $\boldsymbol{t}$ of a single crack. Based on formula (7.1), the direction $\boldsymbol{t}$ of a single crack minimizes the following functional:

$$\mathcal{R}(\boldsymbol{t}) = \sum_{j,l,\omega_k} \left| \mathcal{A}(j,l,\omega_k) - \hat{a}_0^{\varepsilon} - \omega_k^2 \hat{a}_1^{\varepsilon} (\boldsymbol{n}_j \cdot \boldsymbol{t})(\boldsymbol{n}_l \cdot \boldsymbol{t}) \right|^2 .$$

We use 8 and 12 search directions $\boldsymbol{t}_i$ in the situations with Σ_1 and Σ_2, respectively.

The values of $\mathcal{R}(\boldsymbol{t}_i)$ for each of the two cracks Σ_1 and Σ_2 are given in Table 8.3. Note that the values of $\mathcal{R}(\boldsymbol{t}_i)$ are normalized with respect to the maximum value.

l	Value of $\mathcal{R}(\boldsymbol{t}_i)$ for Σ_1	Value of $\mathcal{R}(\boldsymbol{t}_i)$ for Σ_2
1	0.1707	**0.0075**
2	1.0000	0.4356
3	0.2041	1.0000
4	**0.0252**	0.4877
5	0.1707	0.0096
6	1.0000	0.0938
7	0.2041	**0.0075**
8	**0.0252**	0.4356
9		1.0000
10		0.4877
11		0.0096
12		0.0938

TABLE 8.3
Recovering the directions of the small cracks Σ_1 and Σ_2.

Crack	n	$x_1^{(1)}$	$x_1^{(n)}$	Frequency	Imaging functional
$\Sigma^{(m)}$	30	-2	2	$\omega \in [300, 360]$	$\mathcal{I}_{\rm MT}, \mathcal{I}_{\rm KMF}, \mathcal{I}_{\rm KM}$
$\Sigma^{(m)}$	30	-2	2	$\omega = 330$	$\mathcal{I}_{\rm MU}$

TABLE 8.4
Test configuration for $\Sigma^{(m)}$.

From the data in Table 8.3, the estimated tangential direction $\boldsymbol{t}$ of the crack Σ_1 is given by

$$\boldsymbol{t} \simeq \boldsymbol{t}_4, \boldsymbol{t}_8 = (1,0), (-1,0).$$

Similarly, the estimated direction $\boldsymbol{t}$ of the crack Σ_2 is

$$\boldsymbol{t} \simeq \boldsymbol{t}_1, \boldsymbol{t}_7 = \left(\frac{\sqrt{3}}{2}, \frac{1}{2}\right), \left(-\frac{\sqrt{3}}{2}, -\frac{1}{2}\right).$$

Thus, the approach set forth for estimation of crack orientation worked well in this case.

8.2. Imaging of Multiple Small Cracks. Consider the functionals $\mathcal{I}_{\rm MT}$, $\mathcal{I}_{\rm KMF}$, $\mathcal{I}_{\rm KM}$ and $\mathcal{I}_{\rm MU}$ for imaging multiple cracks. We choose for illustration the following example:

$$\Sigma^{(m)} = \{(x - 0.05, -11) : -\varepsilon \le x \le \varepsilon\} \cup \{R_{\pi/4}(x + 0.05, -11) : -\varepsilon \le x \le \varepsilon\}.$$

The test configurations and localization results can be found in Table 8.4 and Fig. 8.7. Note that for $\mathcal{I}_{\rm KMF}, \mathcal{I}_{\rm KM}$, and $\mathcal{I}_{\rm MU}$ there is a peak of much smaller magnitude at the rotated crack (the one on the right). Note that the normalization of the modes in the functional $\mathcal{I}_{\rm MT}$ defined by (3.10) gives a more balanced contrast.

8.3. Robustness With Respect to Measurement Noise. Suppose that the measured data is polluted by a white Gaussian noise so that the SNR is 10dB. In order to test the robustness of the proposed imaging functionals, we consider the imaging of the two-closely located cracks $\Sigma^{(m)}$. The test configuration is the same as in the noiseless case.

Again, in the imaging of $\Sigma^{(m)}$ a peak of much smaller magnitude at the rotated crack (the one on the right) results when using functionals $\mathcal{I}_{\rm KMF}$ and $\mathcal{I}_{\rm KM}$ as shown in Fig. 8.8. Note that the Kirchhoff imaging functionals are not significantly affected by measurement noise. However, the location of the rotated crack via $\mathcal{I}_{\rm MU}$ for $\omega = 330$ can not be identified any more.

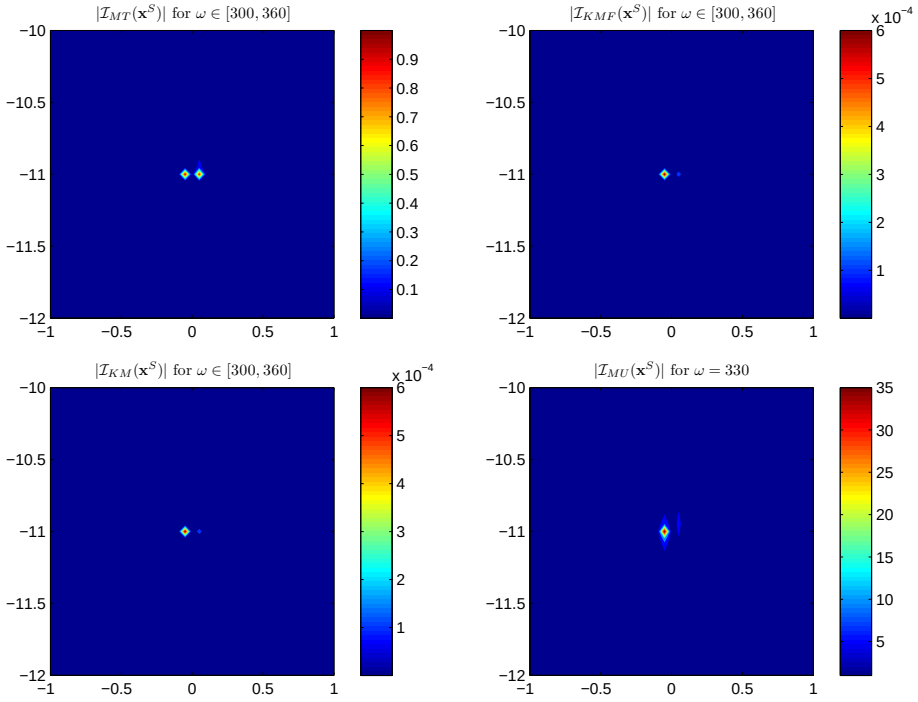

FIG. 8.7. *Localization results for* $\Sigma^{(m)}$ *with* $\mathcal{I}_{\mathrm{MT}}$ *(top left),* $\mathcal{I}_{\mathrm{KMF}}$ *(top right),* $\mathcal{I}_{\mathrm{KM}}$ *(bottom left) and* $\mathcal{I}_{\mathrm{MU}}$ *(bottom right).*

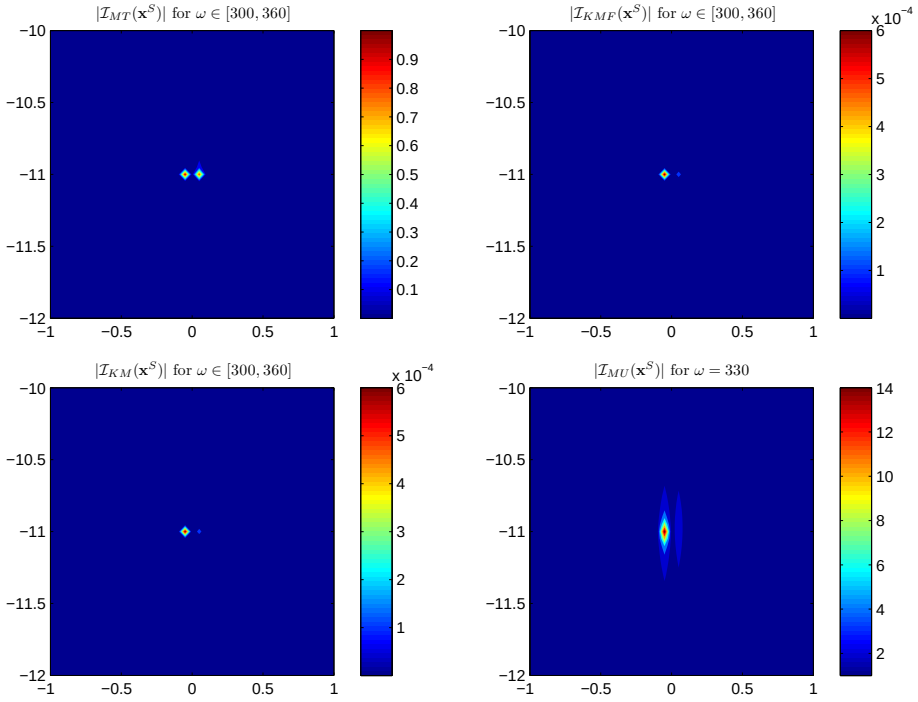

FIG. 8.8. *Localization results for* $\Sigma^{(m)}$ *using* $\mathcal{I}_{\mathrm{MT}}$ *(top left),* $\mathcal{I}_{\mathrm{KMF}}$ *(top right),* $\mathcal{I}_{\mathrm{KM}}$ *(bottom left) and* $\mathcal{I}_{\mathrm{MU}}$ *(bottom right) with* 10 *dB SNR.*

9. Concluding Remarks. We have presented a framework for detection and localization of cracks and inclusions. The approach is based on physical modelling, modelling the formation of the response function using the governing equation for the wave propagation phenomenon and evaluating this via asymptotic techniques. The explicit tests are then based on optimal statistical decision rules in the context when there is additive Gaussian noise. An important aspect of the detection rule is that it is universal in that it depends only on the number of measurements and the prescribed false alarm rate. The approach also addresses the important question of identifying the dimension of the signal space. Our probabilistic approach identifies a Kirchhoff imaging functional as the optimal one in the localization step and we explicitly discuss a notion of resolution. Finally, the asymptotic framework answers the question about what aspects of cracks and inclusions can be estimated based on the measurements and we set forth explicit schemes of estimation of these geometric features. The framework that we have presented can be generalized to the case with cluttered media and the situation with multiple and clustered defaults. This requires to determine the statistical properties of the multi-static response matrix in this framework, using the theory of wave propagation in complex media [21]. Results on this and a more detailed analysis of estimation of geometric features of (extended) cracks and inclusions will be reported elsewhere.

Appendix A. Statistical Test. As in the standard statistical hypothesis testing [18, 24], we postulate two hypotheses and derive a decision rule for deciding in between them based on the measured response matrix.

We define H_0 the (null) hypothesis to be tested and H_A the (alternative) hypothesis:

- H_0: there is no defect,
- H_A: there is a defect.

We want to test H_0 against H_A. Two types of independent errors can be made:

- Type I errors correspond to rejecting the null hypothesis H_0 when it is correct (false alarm). Their probability is given by

$$\alpha := P[\text{accept } H_A | H_0 \text{ true}],$$

  also called the level of significance of the test.
- Type II errors correspond to accepting H_0 when it is false (missed detection) and have probability

$$\beta := P[\text{accept } H_0 | H_A \text{ true}].$$

The success of the test (probability of detection or detection power) is therefore given by $1 - \beta$.

Given the data the decision rule for accepting H_0 or not can be derived from the Neyman-Pearson Lemma which asserts that for a prescribed false alarm rate α the most powerful test corresponds to accepting H_A for the likelihood ratio of H_A to H_0 exceeding a threshold value determined by α.

Neyman-Pearson Lemma: Let Y be the set of all possible data and let $f_0(y)$ and $f_1(y)$ be the probability densities of Y under the null and alternative hypotheses. The Neyman-Pearson Lemma [18, p. 335] states that the most powerful test has a critical region defined by

$$\mathcal{Y} := \left\{ y \in Y \;\middle|\; \frac{f_1(y)}{f_0(y)} \geq \eta_\alpha \right\}, \tag{A.1}$$

for a threshold η_α satisfying

$$\int_{y \in \mathcal{Y}} f_0(y) dy = \alpha. \tag{A.2}$$

If the data is y, we reject H_0 if the likelihood ratio $\frac{f_1(y)}{f_0(y)} > \eta_\alpha$ and accept H_0 otherwise. The power of the (most powerful) test is given by

$$1 - \beta = \int_{y \in \mathcal{Y}} f_1(y) dy. \tag{A.3}$$

Appendix B. Proof of the Asymptotic Formula (2.4). Assume for the sake of simplicity that

$$\Sigma_\varepsilon = \Big\{(x,0) : -\varepsilon \le x \le \varepsilon\Big\}. \tag{B.1}$$

Thus, $\boldsymbol{x}^c = (0,0)$. Suppose also that $c_0 = 1$. Let $\mathcal{X}^\varepsilon$ be defined by

$$\mathcal{X}^\varepsilon = \left\{\varphi : \int_{-\varepsilon}^{\varepsilon} \sqrt{\varepsilon^2 - |\boldsymbol{x}|^2}\, |\varphi(\boldsymbol{x})|^2\, d\boldsymbol{x} < +\infty\right\}. \tag{B.2}$$

Endowed with the norm

$$\|\varphi\|_{\mathcal{X}^\varepsilon} = \left(\int_{-\varepsilon}^{\varepsilon} \sqrt{\varepsilon^2 - |\boldsymbol{x}|^2}\, |\varphi(\boldsymbol{x})|^2\, d\boldsymbol{x}\right)^{1/2},$$

$\mathcal{X}^\varepsilon$ is a Hilbert space.

The following behavior of the Hankel function near 0 holds [25]:

$$-\frac{i}{4} H_0^{(1)}(\omega|x|) = \frac{1}{2\pi} \ln|x| + \tau^\omega + \sum_{n=1}^{+\infty} (b_n \ln(\omega|x|) + c_n)(\omega|x|)^{2n}, \tag{B.3}$$

where

$$b_n = \frac{(-1)^n}{2\pi} \frac{1}{2^{2n}(n!)^2}, \quad c_n = -b_n\left(\gamma - \ln 2 - \frac{\pi i}{2} - \sum_{j=1}^{n} \frac{1}{j}\right),$$

and the constant $\tau^\omega = (1/2\pi)(\ln\omega + \gamma - \ln 2) - i/4$, γ being the Euler constant.

We have the integral representation

$$u_\varepsilon^{(j)}(\boldsymbol{x}) = \hat{G}(\omega, \boldsymbol{x}, \boldsymbol{x}_j) + \int_{\Sigma_\varepsilon} \phi_\varepsilon(y) \hat{G}(\omega, \boldsymbol{y}, \boldsymbol{x})\, d\sigma(y), \quad \boldsymbol{x} \neq \boldsymbol{x}_j, \quad \boldsymbol{y} = (y,0), \tag{B.4}$$

where the density ϕ_ε is the solution in $\mathcal{X}^\varepsilon$ to the integral equation

$$\int_{\Sigma_\varepsilon} \phi_\varepsilon(y) \hat{G}(\omega, \boldsymbol{y}, \boldsymbol{x})\, d\sigma(y) = -\hat{G}(\omega, \boldsymbol{x}, \boldsymbol{x}_j) \quad \text{for } \boldsymbol{x} = (x,0) \in \Sigma_\varepsilon.$$

From (B.3) it then follows that ϕ_ε is the solution in $\mathcal{X}^\varepsilon$ to

$$(-\frac{1}{2\pi}\mathcal{L}_\varepsilon + \mathcal{R}_\varepsilon)[\phi_\varepsilon] = -\hat{G}(\omega, \cdot, \boldsymbol{x}_j) \quad \text{on } \Sigma_\varepsilon,$$

where

$$\mathcal{L}_\varepsilon[\phi](x) = \int_{-\varepsilon}^{\varepsilon} \ln|x-y|\, \varphi(y)\, dy \quad \text{and} \quad \mathcal{R}_\varepsilon[\phi](x) = \int_{-\varepsilon}^{\varepsilon} R^\omega(x,y)\, \varphi(y)\, dy,$$

with

$$R^\omega(x,y) = -\tau^\omega - \sum_{n=1}^{+\infty} (b_n \ln(\omega|x-y|) + c_n)(\omega|x-y|)^{2n}.$$

Set

$$\tilde{\phi}_\varepsilon(x) := \varepsilon\phi_\varepsilon(\varepsilon x).$$

By a change of variables, we get

$$\int_{-\varepsilon}^{\varepsilon} R^\omega(x,y)\phi_\varepsilon(y)\,dy = -\tau^\omega \int_{-1}^{1} \tilde{\phi}_\varepsilon(y)\,dy + O((\omega\varepsilon)^2\ln(\omega\varepsilon)),$$

where $O((\omega\varepsilon)^2\ln(\omega\varepsilon))$ is in the $\mathcal{X}^1$-norm. Analogously to [9], it then follows that

$$\begin{aligned} &-\frac{1}{2\pi}\mathcal{L}_1[\tilde{\phi}_\varepsilon] + C_\varepsilon\Big(-\frac{\ln\varepsilon}{2\pi} - \tau^\omega\Big) + O((\omega\varepsilon)^2\ln(\omega\varepsilon)) \\ &\quad = -\hat{G}(\omega,\boldsymbol{x}^c,\boldsymbol{x}_j) - \varepsilon x\frac{\partial\hat{G}}{\partial x}(\omega,\boldsymbol{x}^c,\boldsymbol{x}_j) + O(\varepsilon^2\omega^2), \end{aligned}$$

where

$$C_\varepsilon^\omega = \int_{-1}^{1} \tilde{\phi}_\varepsilon(y)\,dy.$$

Here $\partial/\partial x$ is the tangential derivative on Σ_ε defined by (B.1). Using the explicit form of $\mathcal{L}_1^{-1}$ as in Lemma 2.1 in [9] yields

$$\begin{aligned} \tilde{\phi}_\varepsilon(y) = \frac{\hat{G}(\omega,\boldsymbol{x}^c,\boldsymbol{x}_j)}{\ln(1/2)\sqrt{1-y^2}} - C_\varepsilon^\omega\frac{\ln\varepsilon + 2\pi\tau^\omega}{\pi\ln(1/2)\sqrt{1-y^2}} - 2\varepsilon\frac{\partial\hat{G}}{\partial x}(\omega,\boldsymbol{x}^c,\boldsymbol{x}_j)\frac{y}{\sqrt{1-y^2}} \\ +O((\omega\varepsilon)^2\ln(\omega\varepsilon)), \end{aligned}$$

and therefore, since $\varepsilon\frac{\partial\hat{G}}{\partial x}(\omega,\boldsymbol{x}^c,\boldsymbol{x}_j) = O(\varepsilon\omega)$,

$$C_\varepsilon^\omega = \frac{2\pi\hat{G}(\omega,\boldsymbol{x}^c,\boldsymbol{x}_j)}{\ln(1/2) + \ln\varepsilon + 2\pi\tau^\omega} + O(\varepsilon\omega).$$

Finally, plugging the expansion of $\tilde{\phi}_\varepsilon$ in (B.4) we get the desired asymptotic formula for $u_\varepsilon^{(j)}$ which is uniform in $\varepsilon\omega$.

REFERENCES

[1] R. Adamczak, A few remarks on the operator norm of random Toeplitz matrices, J. Theor. Probab., DOI 10.1007/s10959-008-0201-7 (2009).

[2] N. I. Akhiezer and I. M. Glazman, *Theory of Linear Operators on Hilbert Spaces*, Vol. 1, Dover, New York, 1993.

[3] H. Ammari, P. Garapon, L. Guadarrama Bustos, and H. Kang, Transient anomaly imaging by the acoustic radiation force, J. Diff. Equat., to appear.

[4] H. Ammari, E. Iakovleva, and D. Lesselier, Two numerical methods for recovering small electromagnetic inclusions from scattering amplitude at a fixed frequency, SIAM J. Sci. Comput. **27**, 130-158 (2005).

[5] H. Ammari, E. Iakovleva, and D. Lesselier, A MUSIC algorithm for locating small inclusions buried in a half-space from the scattering amplitude at a fixed frequency, SIAM Multiscale Model. Simul. **3**, 597-628 (2005).

[6] H. Ammari and H. Kang, *Reconstruction of Small Inhomogeneities from Boundary Measurements*, Lecture Notes in Mathematics, Vol. 1846, Springer-Verlag, Berlin, 2004.

[7] H. Ammari and H. Kang, *Polarization and Moment Tensors: with Applications to Inverse Problems and Effective Medium Theory*, Applied Mathematical Sciences, Vol. 162, Springer-Verlag, New York, 2007.

[8] H. Ammari, H. Kang, and H. Lee, *Layer Potential Techniques in Spectral Analysis*, Mathematical Surveys and Monographs, Vol. 153, American Mathematical Society, Providence RI, 2009.

[9] H. Ammari, H. Kang, H. Lee, and W.K. Park, Asymptotic imaging of perfectly conducting cracks, SIAM J. Sci. Comput., to appear.

[10] G. Bal and O. Pinaud, Time reversal based detection in random media, Inverse Problems **21**, 1593-1620 (2005).
[11] A. P. Berens, NDE reliability data analysis, ASM Handbook, Vol. 17, 689-701 (1989).
[12] L. Borcea, G. Papanicolaou, and C. Tsogka, Adaptive interferometric imaging in clutter and optimal illumination, Inverse Problems **22**, 1405-1436 (2006).
[13] A. Bose and A. Sen, Spectral norm of random large dimensional noncentral Toeplitz and Hankel matrices, Electron. Comm. Probab. **12**, 29-35 (2007).
[14] W. Bryc, A. Dembo, and T. Jiang, Spectral measure of large random Hankel, Markov and Toeplitz matrices, Ann. Probab. **34**, 1-38 (2006).
[15] M. Capitaine, C. Donati-Martin, and D. Féral, The largest eigenvalue of finite rank deformation of large Wigner matrices: convergence and nonuniversality of the fluctuations, Ann. Probab. **37**, 1-47 (2009).
[16] G. Casella and . L. Berger, *Statistical Inference*, Duxbury Press, Pacific Grove, 2002.
[17] S. Chatterjee, Fluctuations of eigenvalues and second order Poincaré inequalities, Probab. Theory Relat. Fields **143**, 1-40 (2009).
[18] A. C. Davison, *Statistical Models*, Cambridge University Press, Cambridge, 2003.
[19] A. Fannjiang and K. Sølna, Broadband resolution analysis for imaging with measurement noise, J. Opt. Soc. Am. A **24**, 1623-1632 (2007).
[20] D. Féral and S. Péché, The largest eigenvalue of rank one deformation of large Wigner matrices, Comm. Math. Phys. **272**, 185-228 (2006).
[21] J.-P. Fouque, J. Garnier, G. Papanicolaou, and K. Sølna, Wave Propagation and Time Reversal in Randomly Layered Media, Springer, New York, 2007.
[22] D. J. Hansen and M. S. Vogelius, High frequency perturbation formulas for the effect of small inhomogeneities, J. Phys.: Conf. Ser. **135**, 012106 (2008).
[23] K. Johansson, Shape fluctuations and random matrices, Comm. Math. Phys. **209**, 437-476 (2000).
[24] S. M. Kay, *Fundamentals of Statistical Signal Processing, Detection Theory*, Englewood Cliffs, Prentice-Hall, 1998.
[25] N. N. Lebedev, *Special Functions and Their Applications*, Prentice-Hall, Englewood Cliffs, 1965.
[26] M. Meckes, On the spectral norm of a random Toeplitz matrix, Elect. Comm. in Probab. **12**, 315-325 (2007).
[27] M. L. Mehta, *Random Matrices*, Academic Press, San Diego, 1991.